



**Politecnico  
di Torino**

**Politecnico di Torino**

Master's degree in Mechanical Engineering  
A.a. 2020/2021  
December 2021

# **Experimental analysis of a car model in 1 to 5 scale**

Supervisors:

Prof. Vigliani Alessandro  
Prof. Bonisoli Elvio  
Dott. Vella Angelo Domenico

Candidate:

Odoardi Davide



# Index

Index.....	1
Abstract.....	3
Introduction.....	4
1. Tests on the suspension springs .....	8
1.1 The springs.....	8
1.2. Berco CM250E .....	9
1.2.1 Testing machine functionalities description .....	10
1.2.2 The test procedure .....	11
1.3. The test.....	12
1.3.1 Stiffness computation.....	13
1.3.2 Test results .....	13
1.4 Test conclusions .....	15
2 GPS data processing.....	16
2.1. Positioning of the GPS receiver and the SCADAS XS on the vehicle .....	17
2.2. The test.....	18
2.2.1 Test1 .....	19
2.2.2 Test2.....	20
2.2.3 Test3.....	22
2.2.4 Test4.....	23
2.3 Data exportation .....	24
2.4. Data post processing .....	25
2.4.1 First algorithm, great-circle distance .....	25
2.4.2 Second algorithm, the haversine formula .....	26
2.4.3 Third algorithm, Matlab Mapping Toolbox .....	27
2.4.4 Precision of the algorithms in distance computation .....	27
2.4.5 Test distance computation comparison .....	29
2.5 Velocity data analysis .....	31
2.5.1 GPS velocities data .....	31
2.5.2 Speed computation by latitude-longitude information.....	32
2.6 Conclusions.....	33
3 Wheels steering angle measurement.....	34
3.1 Losi 5ive steering system.....	34
3.2 Wheel angle measure .....	35
3.3 PXI acquisition, direct electric measure of the steering angle .....	38
3.3.1 PXI acquisition tests.....	39
3.4 Steering system CAD models .....	41
3.4.1 Matlab model .....	41
3.4.2 Adams View model.....	45
3.5 Servomotor angle measure using a potentiometer .....	49
3.6 Wheel angle estimation using the potentiometer data .....	52
4 Vehicle Dynamics .....	55
4.1 Bicycle model. ....	55
4.2 Steering models.....	55
4.3 Triaxial Accelerometers .....	56
4.3.1 RPM estimation.....	57
4.3.1.1 The performed test .....	57
4.3.1.2 Matlab “rpmtrack”. ....	59

4.3.1.3 RPM estimation results .....	63
4.4 IMU .....	63
4.4.1 IMU positioning on the vehicle .....	64
4.4.2 Test performed .....	67
5 Conclusion and future development .....	70
Reference .....	71

## Abstract

The following thesis work focuses on the analysis of the experimental measures coming from a heterogeneous set of sensors mounted on a 1:5 scale car model.

The car model is a Losi 5ive T-2.0, while the sensors used are triaxial accelerometers, an IMU, a GPS and a potentiometer.

The main goal of the experimentation conducted in the laboratory is to extrapolate quantifiable vehicle dynamics parameters used to characterize the vehicle behavior and properties. These parameters are the vehicle positioning, velocities, accelerations, and steering angle measures.

A first chapter is dedicated to the suspension characterization validation. Then the vehicle set-up will be discussed. The thesis continues by dealing with the processing of data acquired by GPS connected to a Siemens SCADAS XS. The GPS allows to find the positioning track record during the outdoor tests and gives a set of data from which the vehicle velocities and orientation can be retrieved.

In a second test phase, the vehicle has been equipped with accelerometers, a potentiometer utilized to measure the steering angle of the vehicle wheels, and an IMU. The accelerometer allows us to find data about the car dynamics. The IMU is mounted instead of the accelerometers during further testing because of its capacity to acquire the constant accelerations and because of the vehicle orientation measure obtained by the built-in magnetometer.

A Simcenter SCADAS XS has been utilized for the acquisition of the data generated by the sensors. All the data post-processing is conducted in Mathworks Matlab, to which two Toolboxes have been added: Mapping Toolbox and Signal Processing Toolbox.

## Introduction

The entire work concerns experimentation activities carried out on a Losi 5ive-T 2.0. The Losi 5ive-T-2.0 is a 1:5 scale, 4WD, radio-controlled Truck. It is a racing scaled vehicle powered by a Zenoah 32cc gasoline pull start engine able to push the vehicle near to the 70 km/h. In the following figure is shown the truck in various angulations.



Figure 1 – Losi 5ive-T 2.0, isometric front view, with and without the cover



Figure 2 – Losi 5ive-T 2.0, isometric rear view, with and without the cover



Figure 3 – Losi 5ive-T 2.0, lateral view, with and without the cover

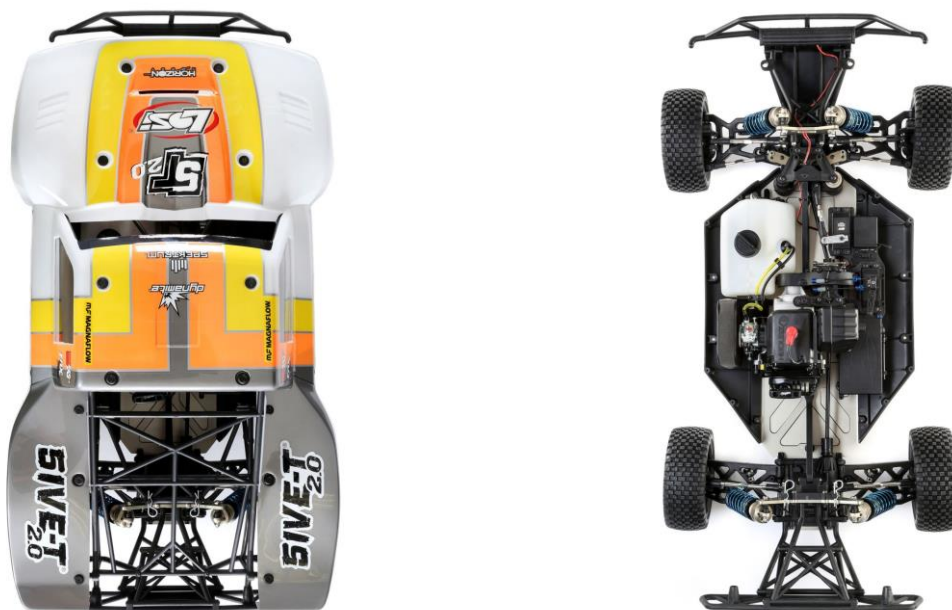


Figure 4 – Losi 5ive-T 2.0, top view, with and without the cover

The vehicle has a net weight of 16 kg, is 965.2 mm long, 527 mm width and 311.1 mm high, with a ground clearance of 50.8 mm. The wheelbase is 609.6 mm, while the wheels have squared pins and a 71.1 mm diameter. The wheels are connected to the body thanks to polycarbonate structural parts and thanks to the oil-filled suspension system. The vehicle chassis is composed by elements in different materials: polycarbonate and a 5 mm thick 6061-T6 aluminum plate. On the metal plate are secured all the internal elements of the vehicle, such as the Zenoah G320 engine, the 2S Li-PO battery, the 800 cc tank, the Spektrum SR600T radio receiver, and the steering system [1]. The vehicle can be controlled by a radio transmitter, in this case a Spektrum DX5 Pro (Figure 5).



Figure 5 – Spektrum DX5 Pro.

The Spektrum DX5 Pro has manual controls for the throttle/brake with a leverage, and a manual steering control with the wheel-shaped element in the front. On its top there is a display with which it is possible to control the vehicle status, the vehicle battery status, and the receiver battery level. In addition, the DX5 Pro allows a precise control on every vehicle's element behavior and allows to modify the vehicle drive response. However, it can be used even without a deep knowing on the various settings available.

Due to the experimental nature of the tests conducted in this thesis work, the vehicle has been started up for the first time. The start-up procedure is well illustrated in a very meticulously way in the user manual [2], only few significant steps will be reported.

The vehicle first start-up procedure could be divided into two macro steps: the transmitter/receiver binding and the vehicle start up.

For what concerns the receiver/transmitter binding must be followed these instructions. First, turn on the transmitter, then the receiver soon after having installed the battery in the vane under the exhaust gas exit. Never do the opposite, uncontrollable vehicle behavior may occur. Second, push the binding button, represented in Figure 6, on the receiver until a blinking light appears. The function “binding” must be selected on the transmitter since is the first start.

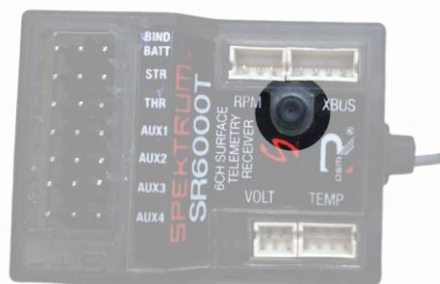


Figure 6 – Spektrum SR6000T receiver, binding button evidenced.

The binding process is concluded when the led stills.



The second macro step concerns the vehicle ignition. The Zenoah G320 needs a mixture of gasoline and 2-cycle oil. A 25:1 ratio gasoline to oil must be used. Gasoline should be 92–98 Octane. Verified the transmitter and the receiver are connected, the engine must be filled with the fuel. To do so, the primer bulb must be pushed until the bulb is filled and the fuel flows through the yellow return line (Figure 7).



Figure 7 – Fuel bulb.

It is now possible to start the vehicle. Set the choke on and pull the start chord in a quick continuous motion (about 3 times) until the engine almost start, then stop. Be careful not to flood the engine with fuel. Do not pull more than 50 cm/20 in or the pull start assembly could damage. Set the choke off and pull the starter chord to start the engine [2]. If the engine is already hot, repeat the procedure above without activating the choke. Now that the vehicle is started, the engine needs two to three minutes in idle to achieve the operating temperature, after that drive slowly the vehicle for about twenty-five minutes to break in the engine.

Now a series of vehicles setting up must be done, such as the engine tuning or the adjusting of the steering and throttle trims but will not be discussed.

# 1. Tests on the suspension springs

In the following chapter will be reported the activities concerning CM250E machinery. CM250E machinery was used to verify the results of the spring stiffness of the Losi 5ive-T 2.0 suspensions obtained by the engineer Pesacane during her thesis work [3]. In particular, CM250E allows the control of the absolute parameters of length and load of the spring from which it is possible to obtain the stiffness and the length variation of the spring. Those data will be used to verify if the procedure adopted in the past for the characterization of the springs can be considered valid. Considering that the past results are strongly coherent with what the literature formulas suggest, we expect to find stiffness value in line with the ones found previously.

## 1.1 The springs

The activity carried out deals with the testing of different type of springs. Each of the springs can be identified by a length and a colour that is representative of its mechanical characteristic.

These springs can be grouped by stiffness or by position in which are mounted, i.e. front or rear springs. The main differences between the mentioned are the length of the springs and the stiffness. In fact, measuring the springs with a caliper, it is found the front springs have an average length of 115 [mm], while the rear ones have an average length of 131 [mm]. For what concerns the stiffness, the front springs have a higher stiffness in respect to rear springs. Moreover, the different colours evidence different stiffness. In fact, there is a step increment of about 200 [N/m] of the nominal value by passing from yellow to orange springs. All these differences can be summarized by the Table 1.1.1 and the Table 1.1.2, integrated with other geometric data found in [3].

Table 1.1.1 – Front springs.








Code	LOSB2964	LOSB2965	LOSB2966	LOSB2967
Colour	Yellow	Blue	Red	Orange
Image				
Nominal Stiffness [N/m]	1877.13	2045.31	2206.50	2487.40
Helix height [m]	0.11513	0.1144	0.11445	0.11638
Helix diameter [m]	0.0353	0.0354	0.0355	0.0356
Number of active spires [-]	6.75	6.8	7	7.25
Number of inactive spires [-]	2	2	2	2

Table 1.1.2 – Rear springs.

Code	LOSB2972	LOSB2971	LOSB2973
Colour	Blue	Red	Orange

Image			
Nominal Stiffness [N/m]	1391.39	1650.07	1837.88
Helix height [m]	0.131	0.13013	0.13128
Helix diameter [m]	0.0352	0.03535	0.0354
Number of active spires [-]	7.5	7.5	7.5
Number of inactive spires [-]	2	2	2

## 1.2. Berco CM250E

The Berco CM250E is the machinery used to perform the test on the springs.



Figure 1.2.1 – Isometric view of the Berco S.p.A. CM250E.

The machine is composed essentially by the body, the leverages system on the right side, the measurement plates and the display.

The geometric characteristics of the machinery are the following:

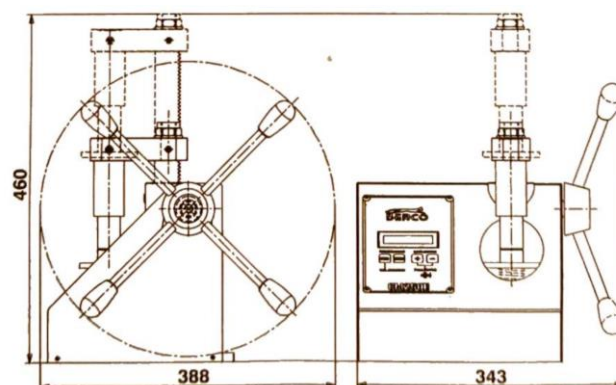


Figure 2.2

Table 1.2.1 – Machine characteristics.

Dimension	Value
Length [mm]	388
Wide [mm]	343
Max height [mm]	460

The geometric characteristics of the spring that can be tested on CM250E are reported in Table 1.2.2.

Table 1.2.2 – Test characteristics.

Property	Value
Max eligible length of the springs [mm]	170
Max eligible external diameter of the springs [mm]	75
Max load [kg]	250
Minimum load [kg]	9
Measure precision of the load [kg]	$\pm 1$
Measure precision of the length [mm]	$\pm 1$

### 1.2.1 Testing machine functionalities description

Once connected to the power supply and turned on by activating the switch on the left side of the machinery, the display shows only two data: the load and the inter distance between the two plates. During the turn on phase the user can select if operating with the metric system or imperial system. For the metric system it is necessary to press and hold the “+” button and soon after activating the turn on switch. For the imperial system the procedure is the same except for the button to press prior the turning on of the machine that is the “-“.

In this phase it is important to establish the *zero* of the measurement, that can be either the completely retracted position, in which the two measurements plates are in contact, or the completely opened position, in which the measurements plates are in the maximum distance possible. Once established the zero of the measuring test phase moving the leverages system on the right, the machine will set the zero to the position desired by pressing simultaneously the “+” and “-“ buttons.

With the rotation the leverages system on the right side of the machine it is possible to push away the measuring plates and prepare the spring for the test using one of the functions of CM250E.

By simply pressing the “*FUN*” (function) button it is possible to access the three different measurement functions of the machine. Once selected the measurement function desired, it is possible to adjust the spring between the plates and begin the measurement using the “*RUN*” button. The functions (or modes) mentioned above are:

1. Free mode: is the very first function available at the device start-up. Once prepared the spring in the test machine it is possible to use the leverages system to excite the spring and read on the display the corresponding values of load and length to the excitation imposed. Taking into account that the excitation comes from a manual operation on the leverage, it is clear that the measures are highly inaccurate, and the values are not easily readable;
2. Length set: this second mode has resemblance in the procedure to the first mode but with a significant difference, that is the data display. In fact, at the begin of this function, the users have to set a desired value of inter distance between the two plate, and when the plates reach that distance, it is possible to read on the display the value of load corresponding to the deformation acquired till the next press of the “*START*” button;

3. Load set: in the procedure is identical to the second mode but this time the users must set a value of load instead of length. When reached the load set prior, it is possible to read the length assumed by the spring till the next press of the “*START*” button.

### 1.2.2 The test procedure

The test was conducted as the manual [4] suggests. The procedure is the following:  
Connection of CM250E to the power supply and activation of the switch.

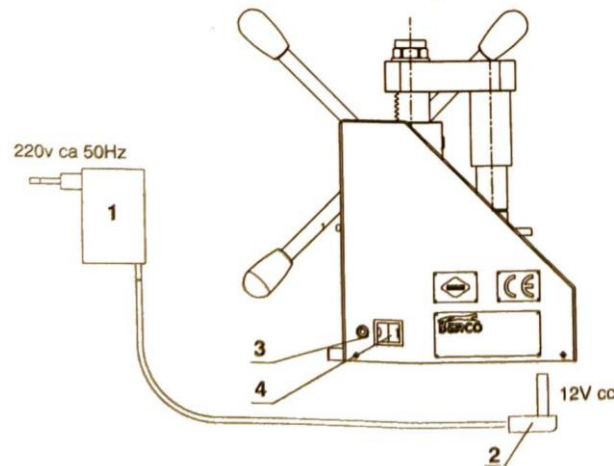


Figure 1.2.2.1.

Selection of the measuring mode by pressing the “*FUN*” button. In our case the test is conducted using the second mode, that is the “*length set*”. With the “+” and the “-” it is possible to set the length value desired.

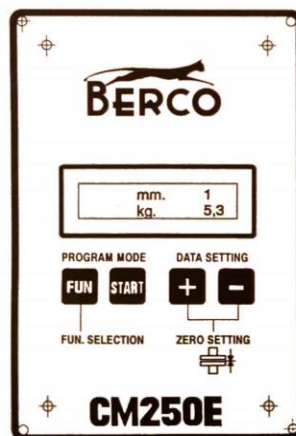


Figure 1.2.2.2.

With the two-measuring plate in contact, press simultaneously the “+” and the “-” buttons to set the zero of the measure. It is possible to set the zero in the total opened configuration even if not explicitly written in the user manual. In this case all the measures taken are negative. Note that the reset operation should be repeated once every 5 to 10 measures to make sure the data collected are not affected by the machine error propagation. It is also recommended to do this procedure every

time the machine reaches the end of the measuring arm elongation without the user have taken care to slow down the arm run near its end.

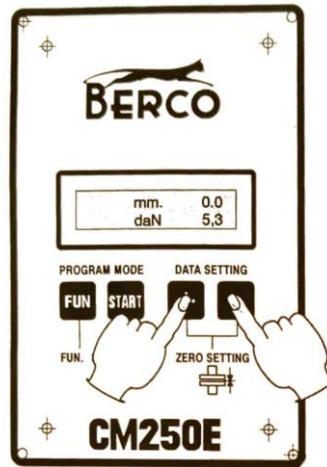


Figure 1.2.2.3.

Using the leverages system on the right side of the machine, it is now possible to raise the upper measuring plate and place a spring in between the plates. Once done, press the button “*START*” and, always using the leverages system, compress the spring till the desired length. During the compression of the spring, a corresponding growing value of the load will be displayed by the machine. When reached the length value previously set, take the spring back in the undeformed configuration. There is no reason to keep the spring compressed, in fact the display will show the test results till the next press of the “*STAR*” button. Make sure to place the spring as centred as possible in between the plates. Do not use the leverages with sudden movements but move continuously to avoid errors in the measurement.

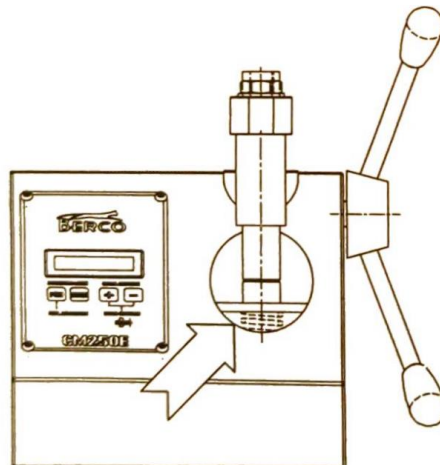


Figure 1.2.2.4.

### 1.3. The test

With the procedure described above, several measures for each of the springs shown in chapter 1 was conducted. For each spring was imposed a deformation to a known length value and then collected the corresponding load measured by the CM250E. For the front springs was imposed a

first deformation till the reach of 110 [mm] and was read the load value corresponding. After five repetition of this first step deformation, were conducted other test compressing the springs till 105 [mm], then 100 [mm], 95 [mm], 90 [mm] and at the end 85 [mm] for a total of 30 load measuring (5 measure for each of the 6 compressing steps). After the measures, were computed the average values of the load data collected and then computed the adjusted average values subtracting 1 [daN] to the average. This adjustment should be done to delete the not null load value present on the start of the machine. Note that if on the turning on of the machine the load value at rest is much higher than 1 [daN] it is mandatory to perform a calibration of the machine. The calibration process needs the specific equipment for the purpose.

### 1.3.1 Stiffness computation

The stiffness computation is performed with the regression function *polyLMS* written by prof. Bonisoli in Matlab®. This function allows to compute the coefficients of a function that fits at best the point measured during the test phase. Moreover, allows to set the origin (0,0) as a constraint for the computation of the function's coefficients. This feature is essential to compute the correct stiffness of the springs because the regression made using only the experimental points lead to a computation of a function in which a null deformation does not correspond to a null load.

The Table 1.3.1.1 shows the stiffness computed, indicating with  $k_{nom}$  the nominal stiffness, and with  $k$  the stiffness adjusted computed by imposing the passage through the origin (0,0) to the function found with the regression.

Table 1.3.1.1.

Springs		Stiffness [N/m]		$\varepsilon$
		Nominal	Computed	
Front	LOSB2966 - Red	2275.56	2286.14	0.46%
	LOSB2967 - Orange	2504.88	2313.40	-7.64%
	LOSB2964 - Yellow	1816.92	1741.48	-4.15%
	LOSB2965 - Blue	2046.24	2011.54	-1.70%
Rear	LOSB2971 - Red	1640.52	1626.24	-0.87%
	LOSB2973 - Orange	1887.48	1893.86	0.34%
	LOSB2972 - Blue	1411.20	1415.42	0.30%

The data are almost equal, except for the stiffness found for the LOSB2967 front orange, that reports a difference between the nominal and the computed stiffnesses higher the 5%.

### 1.3.2 Test results

In this paragraph will be exposed the results obtained testing the springs, shown as plot, where on the y-axis is reported the load expressed in Newton, while on the x-axis is reported the springs deformation in meters.

In the graphs the blue plus sign indicates the experimental load data found during the springs test; the red circle indicates the average load value of the experimental data; the black solid line identifies the function found with *polyLMS* with a null zero order coefficient of the function; the black dash dot line identifies the linear function described by the nominal stiffness.

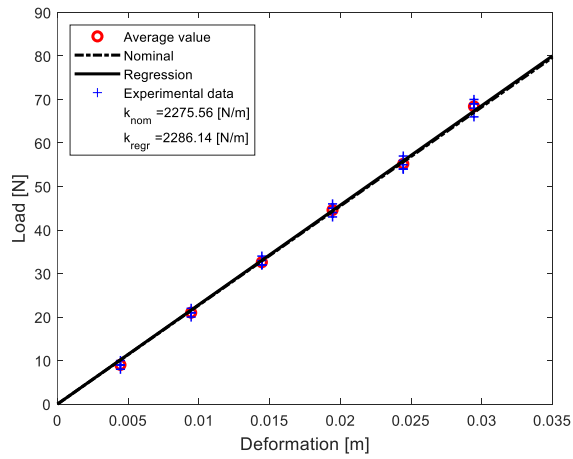


Figure 1.3.2.1 – LOSB2966 Front Red.

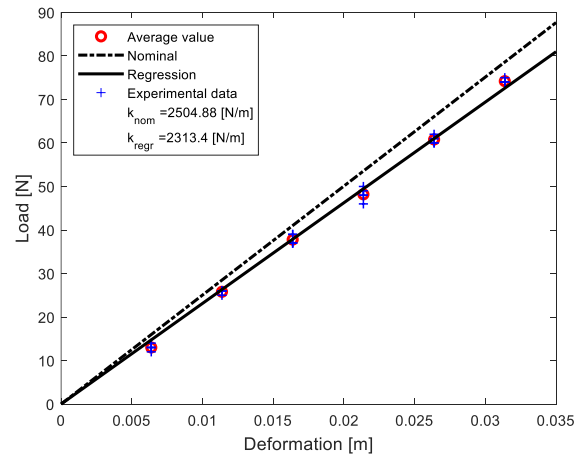


Figure 1.3.2.2 – LOSB2967 Front Orange.

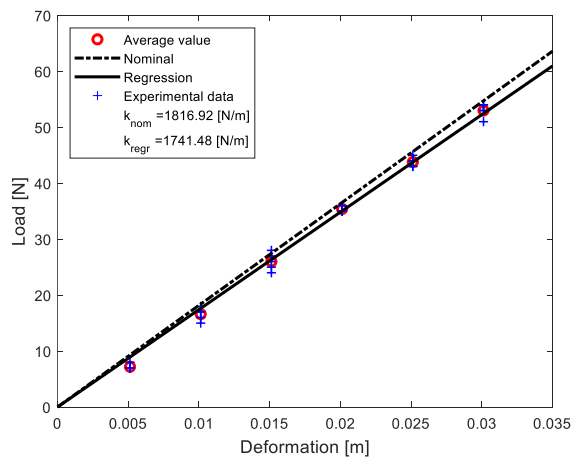


Figure 1.3.2.3 – LOSB2964 Front Yellow.

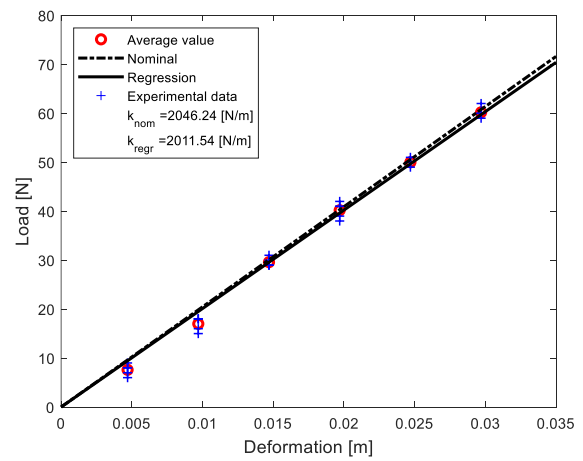


Figure 1.3.2.4 – LOSB2965 Front Blue..

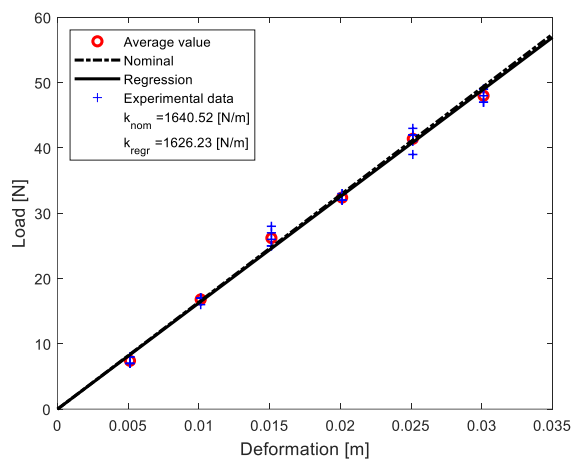


Figure 1.3.2.5 – LOSB2971 Rear Red.

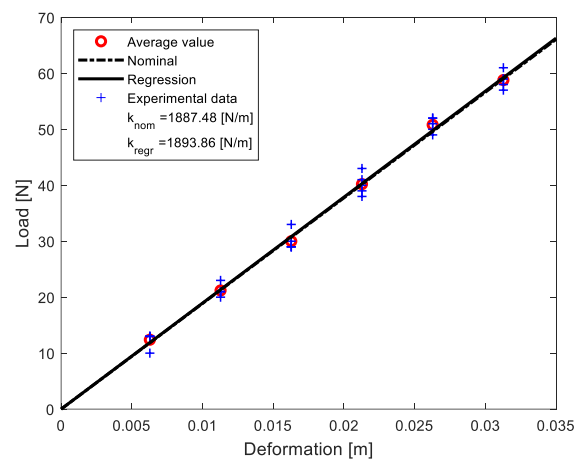


Figure 1.3.2.6 – LOSB2973 Rear Orange.



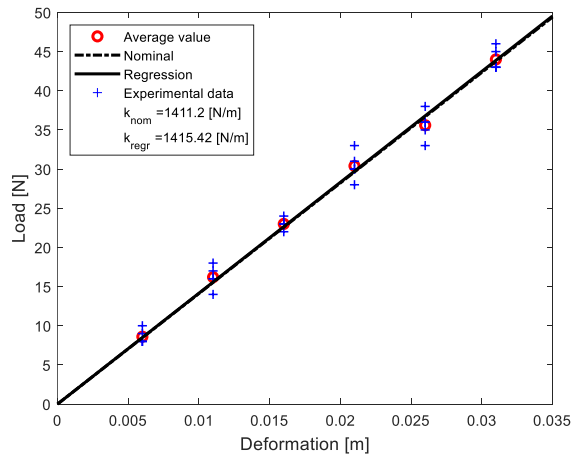


Figure 1.3.2.7 – LOSB2972 Rear Blue.

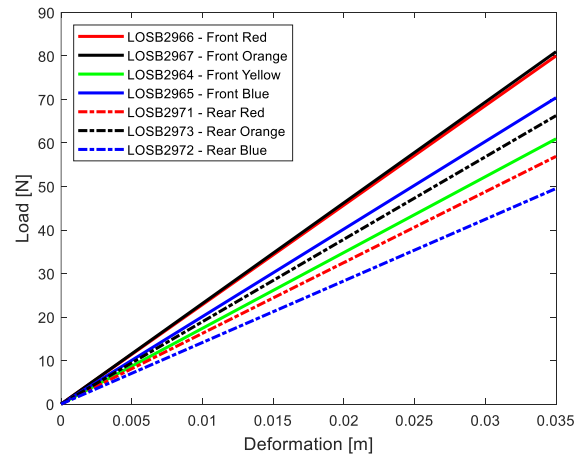


Figure 1.3.2.8 – Springs's comparison.

The Figure 1.3.2.8 is reported to make easier the comparison of the different linear curves found for the different spring characteristics.

From the last graph it is clear that the springs have an incremental increase of the stiffness going to the blue ones to the orange. Increase that is collapsing between the front orange and front red springs that have a very similar computed stiffnesses values.

The stiffness data found are extremely coherent with the nominal ones provided by Losi, in fact in five out of seven cases the error is under the 2% limit. In one case, the LOSB2964 front yellow one, the difference is acceptable being under the 5%. For the last case, the one involving the LOSB2967 front orange spring, it is necessary to perform again the test having found a stiffness not negligibly lower than the nominal one.

## 1.4 Test conclusions

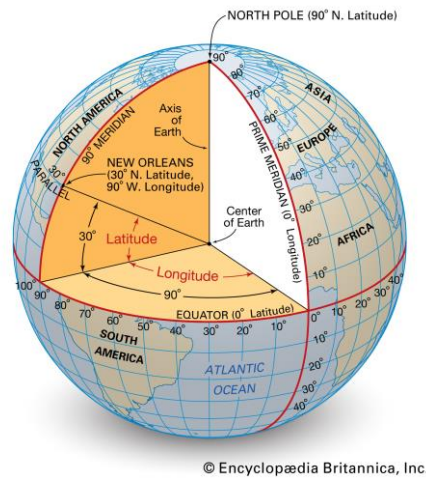
It is reasonable to perform again the tests to the LOSB2967 front orange springs. The reasons are the not negligible difference between the spring nominal stiffness and the computed one, as shown in Table 3.1.1, and the step increase existing between the other springs. Moreover, a new test can be performed also for the LOSB2964 front yellow because of the difference found between nominal and computed stiffnesses is almost about 5%.

## 2 GPS data processing

The aim of this study is to get vehicle velocity data, as well as the instantaneous position. Those data will be utilized for the characterization of the vehicle dynamics once integrated with the acceleration's information.

It is expected to localize the vehicle, define the vehicle's orientation on the globe and study the velocity, in terms of speed and vectorial components.

The Global Positioning System, originally NAVSTAR GPS, is a satellite-based radionavigation system owned by the United States government and operated by the United States Air Force. It is a system that provides geolocation and time information to a GPS receiver. The GPS receiver could be anywhere on or near the Earth, as long as there is an unobstructed line of sight to four or more GPS satellites. Obstacles such as mountains or buildings can block the GPS signal [5]. The GPS can provide several data, such as the latitude, the longitude, and the altitude, but also the instantaneous speed of the vehicle, the North and the East components of the velocity, the velocity with which the GPS sensor is moving in altitude, and the number of satellites in use. The North velocity is the velocity with which the GPS receiver is moving along the north direction, considering positive the velocity that increases the latitude. The East velocity is the velocity with which the GPS receiver is moving along the east direction, considering positive the velocity that increases the longitude. The latitude, the longitude, and the altitude are the positioning information the GPS can retrieve from the satellite. As known, with these data and the local globe radius information, a specific position on the Earth can be univocally identified. The latitude and the longitude are angle measures, while the altitude and the globe radius are linear distances. The longitude is the measure of the angle between the plane passing by Greenwich's meridian and the plane passing by the localized point meridian. The latitude is the angle between the vector perpendicular to the surface of the Earth and the equatorial plane. The altitude is the high of the point relatively to the sea surface. In addition, the latitude and longitude information can be used not only for the spatial identification of a point, but, for example, for the computation of the average speed between two measured points, the orientation of the GPS receiver in respect to the North Pole and the total travel done by the receiver. Obviously, the speed computed by latitude-longitude coordinates needs time information, that can be extrapolate from the characteristics of the GPS receiver. In fact, GPS functioning frequency is 4 Hertz, so can be easily understood that the average speed between two consecutive points of the vehicle can be computed dividing the distance between the points by the 0.25 seconds time interval. Unfortunately, working with latitude longitude system led to a series of obstacles when performing the post-process on the data. The distance computation could be an example. Considering the surface of the Earth an ellipsoid, the distances between two points on the surface of the Earth is not a liner segment, but it is an arch of an ellipsoid. However, simplification can be used. For our purposes, the distances is considered linear due to their very small sizes in comparison with the local Earth radius. Here the necessity to implement a code that allows us to perform a correct post processing from the data acquired.



© Encyclopædia Britannica, Inc.

Figure 2.1 – Latitude and longitude representation.

All these data are collected by a receiver (Figure 2.2) connected to an acquisition data system, in our case the Siemens SCADAS XS (Figure 2.3), through the input port evidenced in the Figure 2.4.



Figure 2.2 – GPS Receiver.



Figure 2.3 – Siemens SCADAS XS.



Figure 2.4 – SCADAS XS, GPS connection port.

## 2.1. Positioning of the GPS receiver and the SCADAS XS on the vehicle

In this paragraph will be discussed the preliminary phases of the tests done with the GPS system, i.e., the positioning on the vehicle and the connection with the SCADAS XS.

The GPS receiver must be mounted on a safe and stable place of the vehicle and, at the same time, a place that allows an easy connection with the acquisition system, i.e., the SCADAS XS. In addition, the GPS receiver cannot work on its own, but it needs an antenna. Usually, the antennas are iron plates to which the GPS receiver can connect magnetically. The plate chosen for the test is an iron plate large as much as the GPS receiver and long 24 centimeters. The position found for the GPS receiver that fits all the necessities explicated above is on the front of the vehicle, in correspondence

of what is used to be the hood on a real size car. The SCADAS XS it is placed on the rear of the vehicle. In Figure 2.1.1 can be easily found the positioning of the equipment on the Losi 5ive T 2.0.

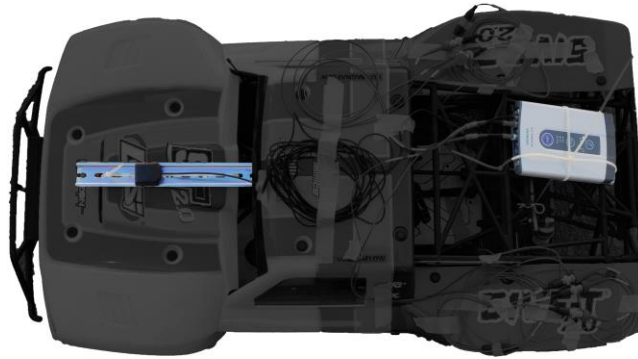


Figure 2.1.1 – GPS receiver and SCADAS XS position on the Losi 5ive T 2.0

On the left side of the Figure 2.1.1 is it possible to find the GPS receiver mounted on the iron plate antenna, while on the right of the same figure the SCADAS XS can be found. Once checked it is all steady on the vehicle, the tests are ready to start.

## 2.2. The test

For the test phase were collected data in different situations: vehicle stationary, vehicle moving in linear path, vehicle moving in a round path, vehicle moving in mix path. For each of these tests were collected data for about 60 seconds. To collect the data, it is important to set in a right way the acquiring system; the SCADAS XS in fact needs a pre configuration. The setup of the SCADAS XS can be done through the companion app in the Android tablet associated, thanks to which, a new test temple can be created. The temple contains the information about the signals are wanted to be acquired and the identification of the signals. The acquisition is stored in the SCADAS XS storage and can be exported by using a micro-sd card. The app on the tablet has a great importance also for the possibility to live check the results the test is producing, allowing a more direct and immediate approach on the experimentation. For our tests it is expected to collect very close values of points coordinates due to the vehicle's low speed. This situation led to difficulties to the post process for the interferences between the localization system errors and the motion of the vehicle in a 0.25 second time interval. This aspect must be considered in the choice of the method used to extrapolate the distance travelled by the vehicle. The tests are performed in the parking lot beside the DIMEAS laboratory, as can be seen in the Figure 2.2.1 and Figure 2.2.2.

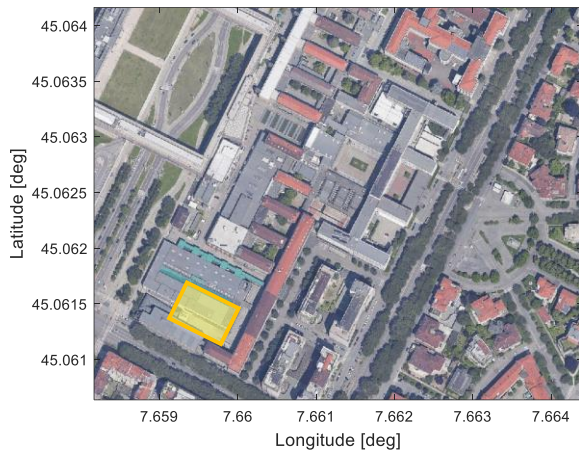


Figure 2.2.1 – Test location.

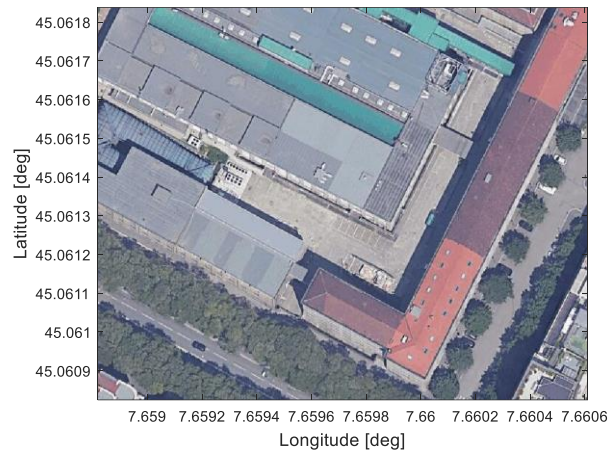


Figure 2.2.2 – Test location, zoomed view.

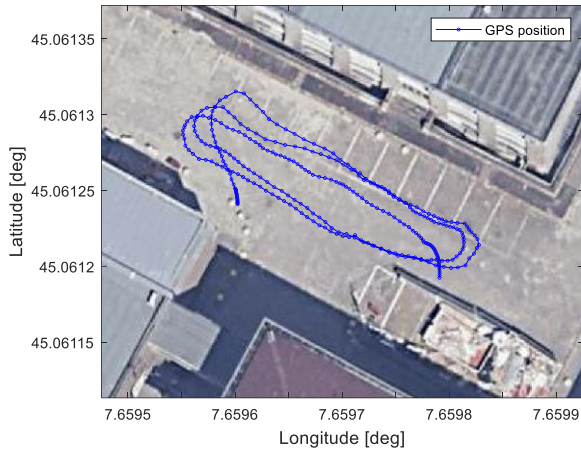
The choice of the test location is subject to some functional condition due to the GPS limitation. The tests must be performed in an open space and possibly far from possible satellite obstacles, such as high buildings.

In the following paragraphs will be shown few representative tests. There are approximately fifty tests' acquisition, but for the positioning problems and velocity computation only few have been selected. The data shown in the graphs are the data directly acquired by the SCADAS XS, except for the map plots in which a little post process is needed to understand the positioning data acquired.

### 2.2.1 Test1

The test “confl\_andata\_e\_ritorno\_001” is the first one taken. The Losi 5ive has been driven in a pseudo elliptic path useful to acquire data both in the curve and during the straight. The Figure 2.2.1.1 shows the positions during the time assumed by the Losi 5ive-T 2.0 in a latitude-longitude system coordinates.

In Figure 2.2.1.2 are plotted the number of active satellites during the test. The minimum number of active satellites useful to retrieve a position on Earth is four. However, with only four active satellites the precision is definitively a critical issue. The number of active satellites should be over or equal to six; the best results are obtained for eight or nine. The active satellites number is directly related to the position assumed over time by the vehicle, but also influences the velocity computation. Considering that the coordinates come from the triangulation of the active satellites' information, if the number of the active satellite changes during the test, there could be the possibility to have instantaneous variation in the GPS position. Those instant variation influences the distance travelled and the velocity computed. That is why it is necessary the time plot of the active number of satellites. If a sudden variation of the velocity or the position is spotted, must be checked if the number of satellites is changing in that time, and correct that information in the post process phase. It is interesting to note that the active satellites number changes when the vehicle speed changes from high to low and vice versa.



Maps data: Google, ©2021, Images ©2021 Maxar Technologies

Figure 2.2.1.1 – Test location.

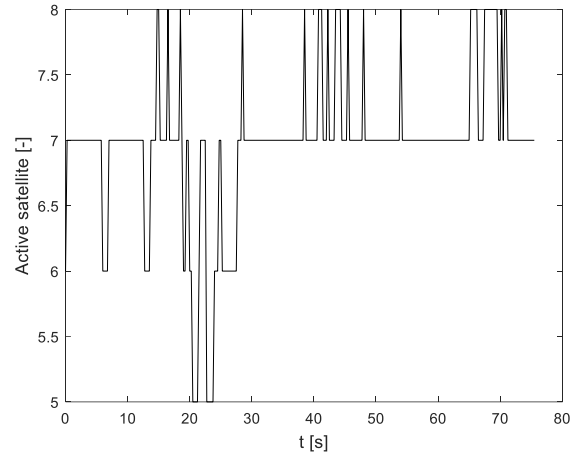


Figure 2.2.1.2 – Active GPS satellites.

In the Figure 2.2.1.3 are plotted the velocity components that will be explained in the paragraph 2.5.1. As expected, the up velocity has a tight variation range since the tests are performed in a planar environment. The three components have negative values because of the orientation of the vehicle: if the vehicle is moving in a southwest direction, both the North velocity and the East velocity will be negative.

The Figure 2.2.1.4 shows the speed with which the vehicle is moving. It represents the velocity magnitude, namely the speed, with which the vehicle is moving. That is why it is always positive.

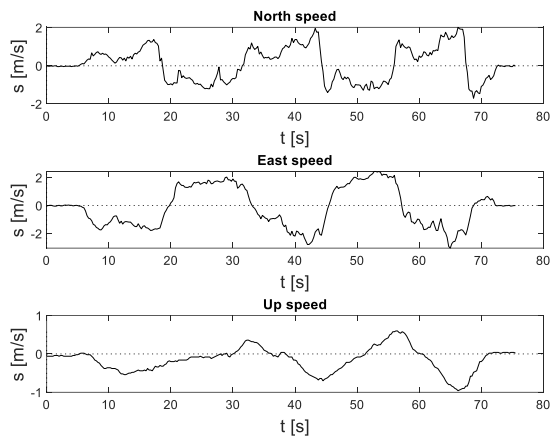


Figure 2.2.1.3 – Velocity components.

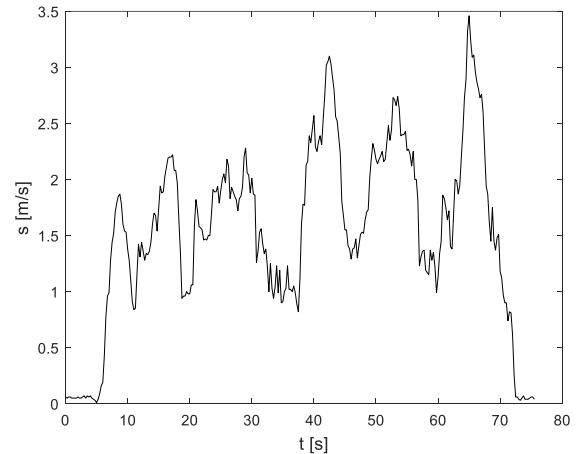


Figure 2.2.1.4 – GPS speed.

## 2.2.2 Test2

The test “conf1\_andata\_e\_ritorno\_002” highlights the GPS imprecision in retrieving coordinates if there are obstacles in the sight between the GPS receiver and the satellites. The Figure 2.2.2.1 shows the coordinates problem: the path travelled by the vehicle is shifted about ten meters in the southwest direction. This shift is due to the relative low number of active satellites at the beginning of the test, as shown in Figure 2.2.2.1, because of the closeness with the Politecnico building. The shift could not be a criticism if there was not the position correction done by the GPS. It happens that if there is a rise in the GPS precision, due to the remoteness with obstacles or due to the active



number of satellites change, the GPS receiver tends to correct the positioning acquisition. This behavior is shown in Figure 2.2.2.2, where it is possible to see a straight segment in the northeast direction in a straight path in the northwest direction. This correction occurred while the vehicle was in a stationary position; this means that while the vehicle was still, the GPS acquired a fictitious movement. There are two main ways to avoid this fictitious movement. The first consists in waiting a couple of minutes allowing the GPS receiver to correct the position before starting the test. If some positioning errors persists, can be implemented a code that detects this error and corrects the position. The first method is by far the easiest and gives the most precise results. That is because no external intervention is needed, so the localization precision is determined by a preconfigured system.

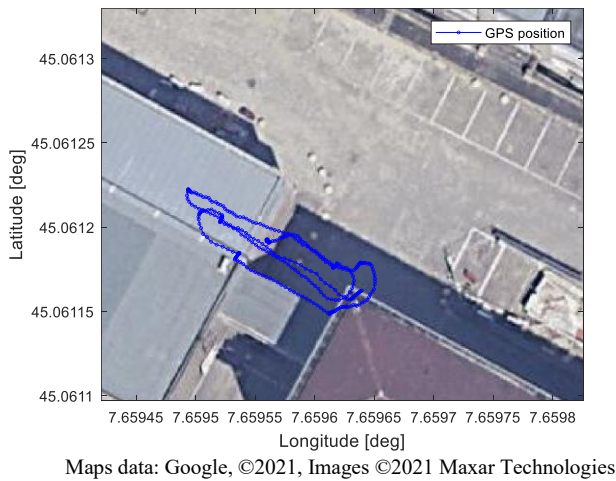


Figure 2.2.2.1 – Test location.

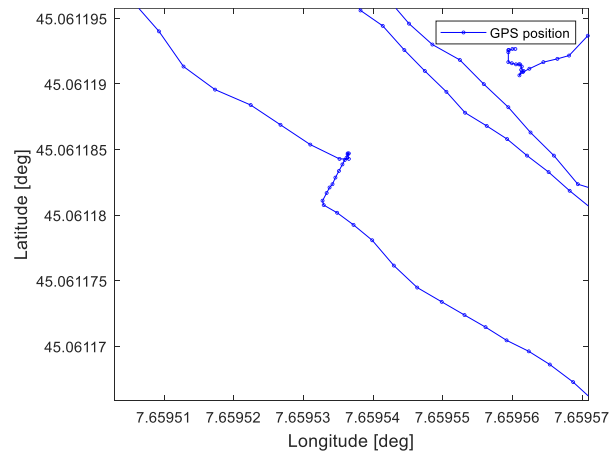


Figure 2.2.2.2 – Test location, zoomed view.

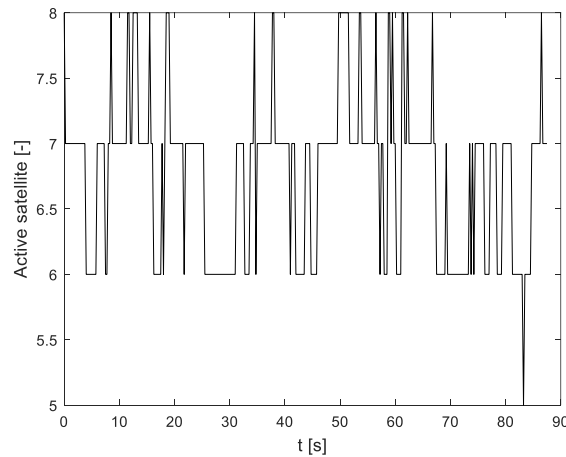


Figure 2.2.2.3 – Active GPS satellites.

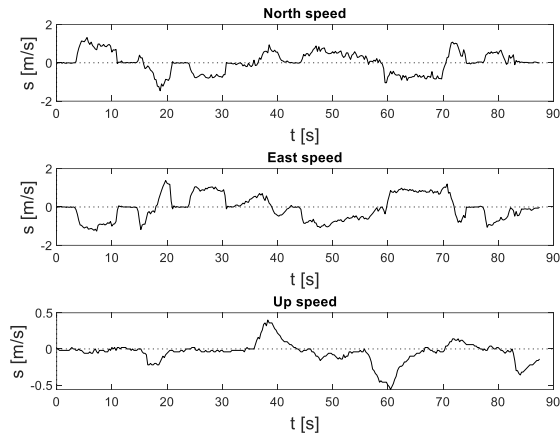


Figure 2.2.2.4 – Velocity components.

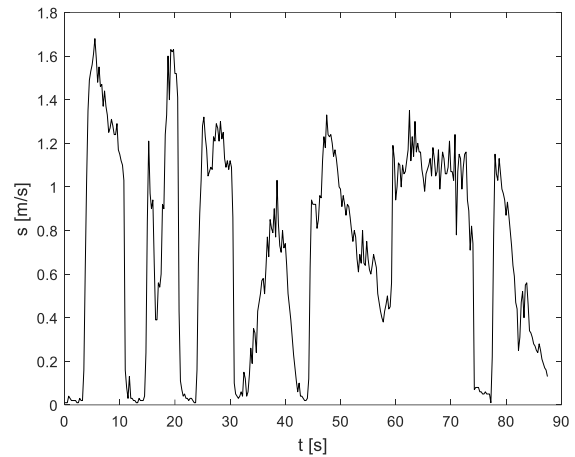


Figure 2.2.2.5 – GPS speed.

### 2.2.3 Test3

The test “confl\_cerchio\_antiorario\_001” is conducted making the car move in an almost circular path. As happened for the previous tests, the initial position suffers of an error of about three meters, even if the initial active satellites are more than enough for a precise localization. This time the position correction is not appreciable from the plot. Having experienced from the past test that the correction occurs while the vehicle is still, there is a high probability that the combination of a closed and small path did not permit at all the position correction.

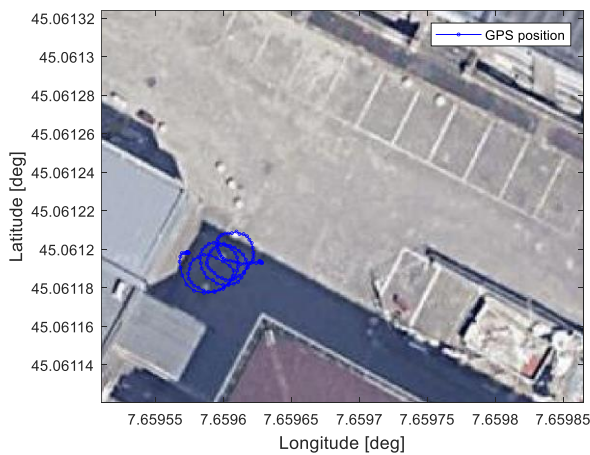


Figure 2.2.3.1 – Test location.

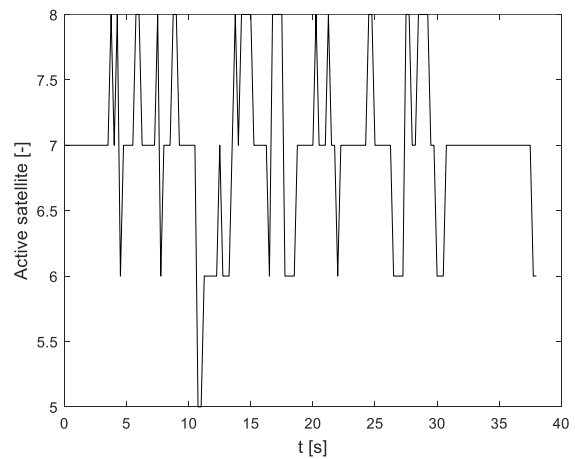


Figure 2.2.3.2 – Active GPS satellites.

An interesting note about this test is that the almost constant speed with which the vehicle travelled the circular path is evidenced by the Figure 2.2.3.3, in which the North speed and the East speed have an oscillatory trend.



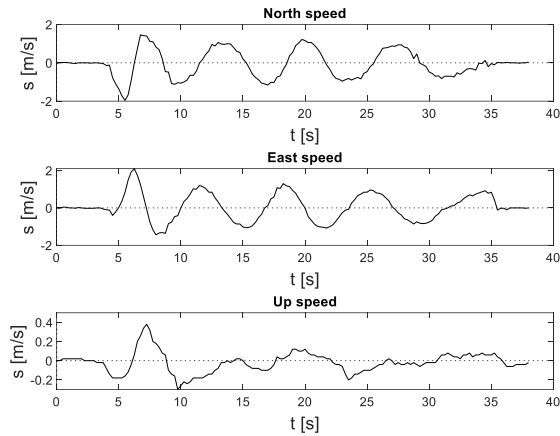


Figure 2.2.3.3 – Velocity components.

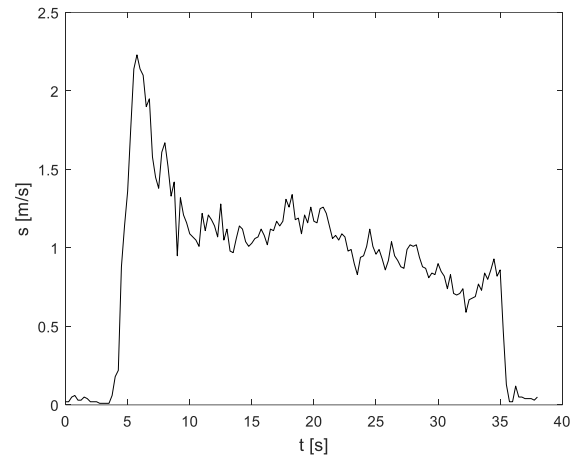


Figure 2.2.3.4 – GPS speed.

## 2.2.4 Test4

The tests “conf1\_fermo\_001” shows in an unambiguous way the position correction process. During the test the vehicle remains still, but still the GPS acquired a movement. The good aspect about this fictitious movements is that introduces speeds errors that are almost null, as can be seen in Figure 2.2.4.4. The maximum range in which the speed changes is 0,09 m/s. Imaging that this fictitious speed is introduced in the test in which the vehicle is moving, the overall error would be in the zero to five percent; that is a reasonable error to accept considering the low speeds the Losi 5ive is subjected.

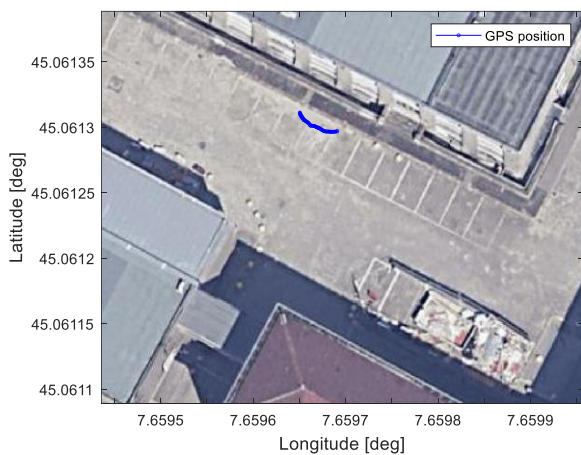


Figure 2.2.4.1 – Test location.

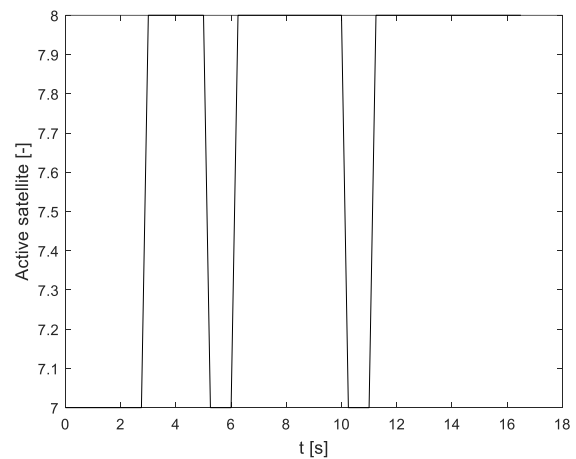


Figure 2.2.4.2 – Active GPS satellites.

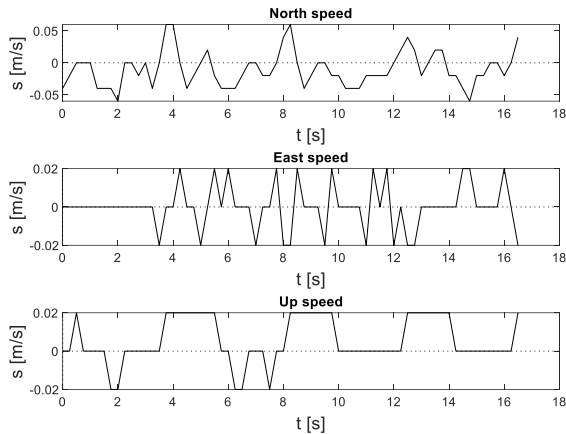


Figure 2.2.4.3 – Velocity components.

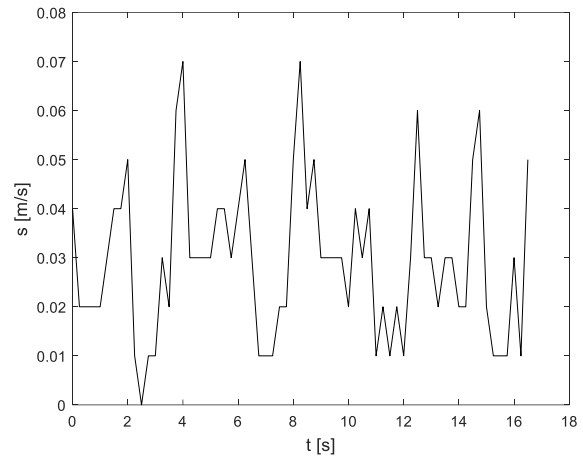


Figure 2.2.4.4 – GPS speed.

## 2.3 Data exportation

As already mentioned, during the tests, the data are collected with the Simcenter SCADAS XS and exported into Matlab files. The data collected by the SCADAS XS during the test are stored into the SCADAS XS storage in the “.sdf” format and can be exported in a PC through the micro-sd card. Although the post process is feasible in TestLab Siemens’s software, for our purposes this software will be used only for the file conversion from “.sdf” to project file “.lms” and then to Matlab “.mat”. During the exportation, the data are organized into a structure containing six signals numbered from 0 to 5. Each signal contains two channels, one dedicated to the time acquisition and one to the physical quantity it is wanted a measure, that could be accelerations, angle coordinates, elevation coordinates, velocity information. Note that the dimension reported into the exported files are valid only if the number associated with the dimension is multiplied by the unit transform factor, available inside the signal information. If the unit transform factor is equal to 1, the measure reported is in the dimension expressed, otherwise is scaled, or not reported in the right dimension. For example, the angle data dimension reported is degrees, but indeed the measures are reported in radians with a unit transformation factor equal to  $\frac{180}{\pi}$ . The data export is organized as expressed in Table 2.3.1.

Table 2.3.1 – Signals.

Signal	x-channel	y-channel	Column	Unit transformation factor
Signal_0	Time [s]	Accelerations [g]	1: $\ddot{x}_1$	0.1020 to obtain [m/s <sup>2</sup> ]
			2: $\ddot{y}_1$	
			3: $\ddot{z}_1$	
			4: $\ddot{x}_2$	
			5: $\ddot{y}_2$	
			6: $\ddot{z}_2$	
Signal_1	Time [s]	Angle coordinates [rad]	1: Latitude	57.2958 to obtain [deg]
			2: Longitude	
Signal_2	Time [s]	Elevation coordinate [m]	1: Altitude	1 to obtain [m]

Signal_3	Time [s]	Local velocities [m/s]	1: East velocity	1 to obtain [m/s]
			2: North velocity	
			3: Up velocity	
Signal_4	Time [s]	Number of satellites [-]	1: Number of satellites	1 to obtain [-]
Signal_5	Time [s]	Absolute speed [m/s]	1: Speed	3.6 to obtain [km/h]

Note that the data export signal organization above is valid only for the cable connection configuration in test. The Signal\_0 data exists because during the GPS positioning tests are collected data coming from two triaxial accelerometers connected to one of the SCADAS XS LEMO connector.

## 2.4. Data post processing

The first step for the data analysis is to export the data acquired by the SCADAS XS to a PC and then, with the help of Siemens Test.Lab software, export those data in “.mat” files. At the end process the information contained in those “.mat” files can be processed in Matlab.

During the post processing, several algorithms have been written and evaluated to find the more precise way to elaborate the GPS data. In particular, three major algorithms have been written, each of them based on a different latitude longitude study approach.

The first algorithm has been written in the base of the great-circle distance theory; the second algorithm is based on the Haversine formula; the third uses an integrated Matlab tool, the Mapping Toolbox.

### 2.4.1 First algorithm, great-circle distance

The first algorithm developed in Matlab takes into account the concept of great-circle distance, also known as orthodromic distance or spherical distance. It represents the shortest distance between two points on the surface of a sphere, measured along the surface of the sphere (as opposed to a straight line through the sphere's interior). The first step to determine this distance is to compute the angular distance between the points with the formula [6]:

$$\gamma = \arccos(\cos(\Delta LON) \cos(LAT_1) \cos(LAT_2) + \sin(LAT_1) \sin(LAT_2)) \quad (2.4.1.1)$$

With:  $\Delta LON$  the difference between the longitude coordinates of the points,  $LAT_1$  and  $LAT_2$  the latitudes of the point 1 and 2.

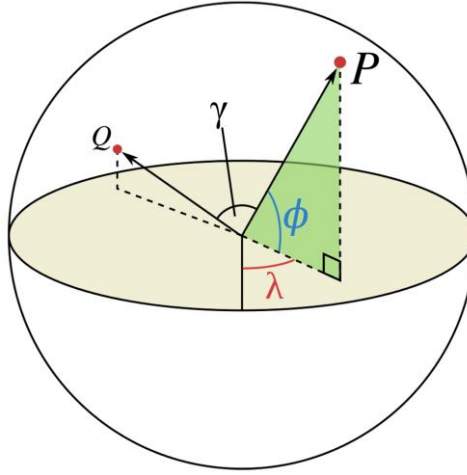


Figure 2.4.1.1 – Graphic representation of the eq (2.4.1.1) elements

Multiplying  $\gamma$  for the average Earth radius between the two points, can be computed the spherical distance expressed in meters. The vehicle total travel can be computed as the sum of all the orthodromic distances computed for all the coordinates collected by the GPS. It is possible to introduce the simplification of the average radius computation thanks to the proximity of the two points from which it is wanted to extrapolate the distance. A different procedure must be considered if the aim were to calculate the distance between the points P and Q of the Figure 2.4.1.1.

This method, however, have some critical issue. The first is that the eq. (2.4.1.1) is valid for spherical geometries, while the Earth has a geoid shape. This is not actually a critical problem because the small errors given by the small distances measured do not discriminate in an appreciably way the choice of the best results code. What put in evidence the weakness of this first method is the arccosine and the floating-point precision on computer systems. Regarding the arccosine, the problem comes when the position of the vehicle is stationary. In fact, in these cases, the argument of the arccosine function is greater than 1, resulting to the computation of complex number in Matlab code. For what concerns the floating-point precision, can be made rounding errors when analyzing distances between very close points, even if in modern computers those rounding errors should not be serious.

## 2.4.2 Second algorithm, the haversine formula

The haversine formula, eq. (2.4.2.1) can be used to compute in a better and more accurate way the spherical distance between two points. This formula allows to overtake the limits of the formula expressed in eq. (2.4.1.1) because the haversine formula is better conditioned for small distances. This means that small errors led to small changes in the output of the function, resulting in a more accurate algorithm. With the haversine formula it is possible to compute the angle distance between the two points in study, then the orthodromic distance can be computed multiplying the angle found with haversine formula by the Earth average radius between the two measured points.

$$\gamma = 2 \arcsin \sqrt{\sin^2 \left( \frac{\Delta \phi}{2} \right) + \cos \phi_1 \cos \phi_2 \sin^2 \left( \frac{\Delta \lambda}{2} \right)} \quad (2.4.2.1)$$

With:  $\phi$  representing the latitude coordinate,  $\lambda$  representing the longitude coordinates.

In the eq. (2.4.2.1) the haversine function has been written in explicit form to not introduce complexity to the text. In fact, the haversine function corresponds to:

$$hav(\theta) = \sin^2\left(\frac{\theta}{2}\right) \quad (2.4.2.2)$$

That will make the eq. (2.4.2.1)  $\gamma = 2 \arcsin \sqrt{hav(\Delta\phi) + \cos \phi_1 \cos \phi_2 hav(\Delta\lambda)}$  (2.4.2.3)

Having written the haversine function in the explicit form allows us to make easier the following step. The haversine formula can be slightly improved for Matlab code trying to obtain an arctan instead of the arcsin. Referring to the trigonometric transformation it is possible to write:

$$\arcsin(x) = 2 \arctan\left(\frac{x}{1 + \sqrt{1 - x^2}}\right) \quad (2.4.2.4)$$

The equation eq. (2.4.2.1) can be transformed in:

$$\gamma = 4 \arctan\left(\frac{\sqrt{\sin^2\left(\frac{\Delta\phi}{2}\right) + \cos \phi_1 \cos \phi_2 \sin^2\left(\frac{\Delta\lambda}{2}\right)}}{1 + \sqrt{1 - \sin^2\left(\frac{\Delta\phi}{2}\right) - \cos \phi_1 \cos \phi_2 \sin^2\left(\frac{\Delta\lambda}{2}\right)}}\right) \quad (2.4.2.5)$$

The choice to transform the arcsine to arctan allows to use the Matlab function atan2, that brings important advantages: allows to avoid the use of the arcsine or arccosine that can lead to complex number; returns a correct and unambiguous value for the angle  $\theta$  when converting from cartesian coordinates (x, y) to polar coordinates (r,  $\theta$ ).

A further step could have been using the Vicenty's formula, valid for a sphere. Like the haversine formula, the Vicenty's formula allows to compute the distance between two points on a spheric surface, measured in angle, but does not suffer from rounding errors in the case of distance computation for antipodal points. Considering the small distances taken into account during the tests, was chosen to stay with the haversine formula and not implement the Vicenty's one.

### 2.4.3 Third algorithm, Matlab Mapping Toolbox

A third method is found using the Matlab Mapping Toolbox. Generally, this toolbox is not included with the standard installation of Matlab, but it is necessary to install it in a second moment. This toolbox can be found in Mathworks website or directly in the "Add-Ons" menu in Matlab.

This toolbox relieves the user to implement algorithms to calculate the orthodromic distance and gives specific functions to solve any map related problem. In particular  $\gamma$  can be simply computed by the Matlab function "distance" giving as the argument of the function the latitude-longitude coordinates and receiving as output  $\gamma$  in radiant or degrees, while the spheric distance can be computed using "rad2km" giving  $\gamma$  as the argument of the function.

### 2.4.4 Precision of the algorithms in distance computation

A simple and quick way to establish if the codes implemented in Matlab are correct in distance and travel calculations, is to compare those algorithms with a reliable source, that is found in Google

Maps. Google Maps allows the user to set two points in the space identified by latitude longitude coordinates and know the distance between those two points. It is also possible to set a path constituted by several point and extrapolate the total distance of the path. The procedure is straight forward: with a right click on the map it is possible to know the point coordinates and the orthodromic distance between two consecutive points. If there are more the two points, Google Maps also plots the total distance as the sum of the consecutive orthodromic distances between the chosen points. These coordinates recording procedure was repeated till the registration of nine points, represented in Figure 2.4.4.1 and stored in Matlab in vectors.

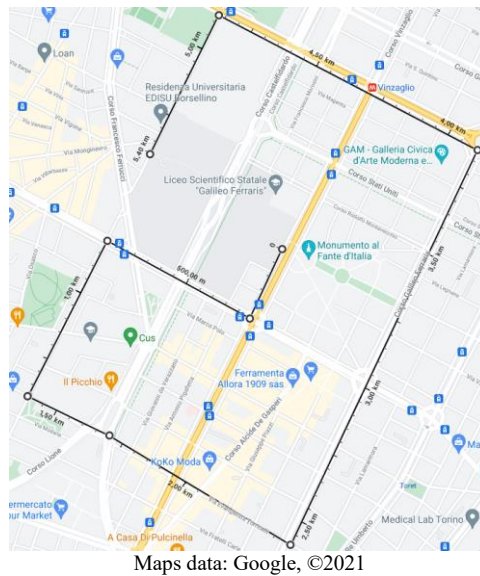


Figure 2.4.4.1 – Google Map plot of the reference path

The codes implemented in Matlab are considered valid if the difference with the reference is under the 5%.

The algorithms produce convincing results as shown in Figure 2.4.4.2 and Figure 2.4.4.3.

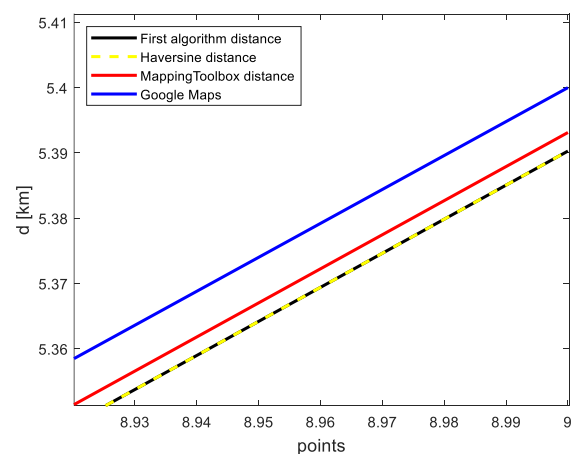
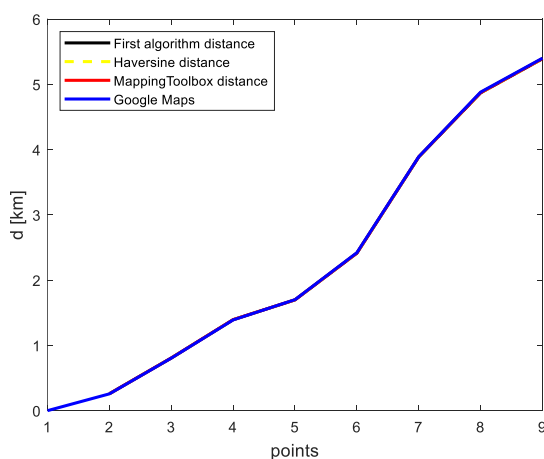


Figure 2.4.4.2 – Distance computation. Figure 2.4.4.3 – Distance computation, zoomed view.

Note that in the plots there should be only points and not lines. The lines are represented only to give more readability to the figures. As can be seen in Figure 2.4.4.2 and Figure 2.4.4.3 the three algorithms compute distances values in line with those read on Google Maps, with deviations under

the 0.18%, far below the 5% acceptable limit. The 0.18% error corresponds in difference below the 1.8 meters for 1 kilometer.

Once the validity of the codes has been verified for large scale distance and low points acquired, it is important to check how those codes behave in short scale distance with a larger number of points coordinates acquired, not only in terms of distances, but also in terms of average speed computation.

From now on, when calling a distance computation, the distance computed by the Mapping Toolbox algorithm is taken as reference.

## 2.4.5 Test distance computation comparison

In all the tests performed, the Mapping Toolbox algorithm and the haversine algorithm gives very close results. The haversine tends to a minor underestimation of the distance travelled but must be considered the entity of the error is in the millimeters field. As expected, the “first algorithm”, does not always give good results. When the vehicle is moving with a velocity over the 2 m/s and never stops, the “first algorithm” computes the distances with an error lower than 2%. This is the situation of the test “conf1\_andata\_e\_ritorno\_001”, as evidenced by the Figure 2.4.5.1 and Figure 2.4.5.2.

However, if the vehicle moves with small velocities, under to 2 m/s, and stops during the test, the “first algorithm” compute distance values with errors in the order of the 10%. This situation can be seen in the Figure 2.4.5.2 and Figure 2.4.5.3 representing the test “conf1\_andata\_e\_ritorno\_002”.

The “first algorithm” produces such a different value because it has not a good precision in the distance calculation between two very close points. When the vehicle is moving with a low speed, the Mapping Toolbox and the haversine algorithms still compute distances even if in the sub meters range. The first algorithm tends to set to zero those little distances, so in the computation of the total distance travelled it is missing some information. Those are characteristics that derives directly from the  $\gamma$  computation, already discussed in the previous paragraphs.

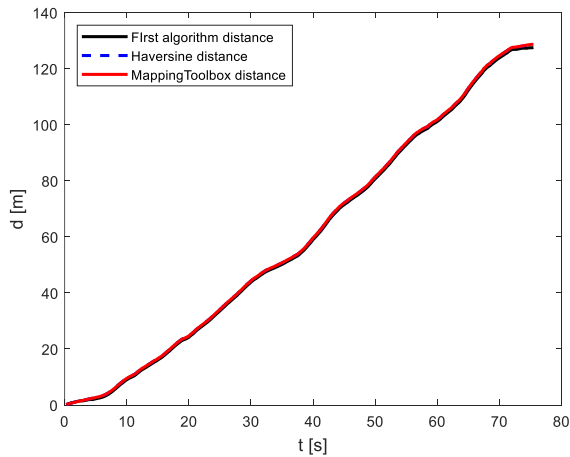


Figure 2.4.5.1 – conf1\_andata\_e\_ritorno\_001.

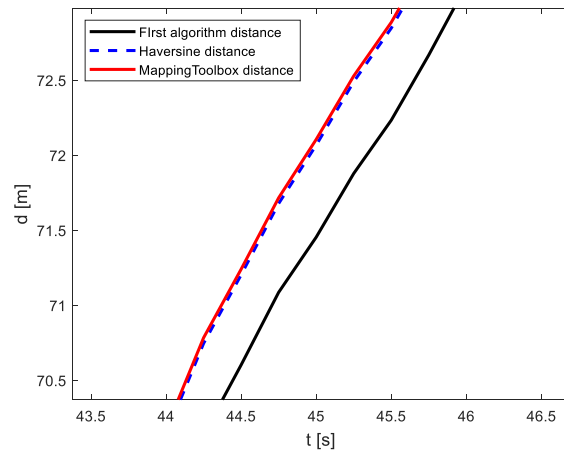


Figure 2.4.5.2 – conf1\_andata\_e\_ritorno\_001.

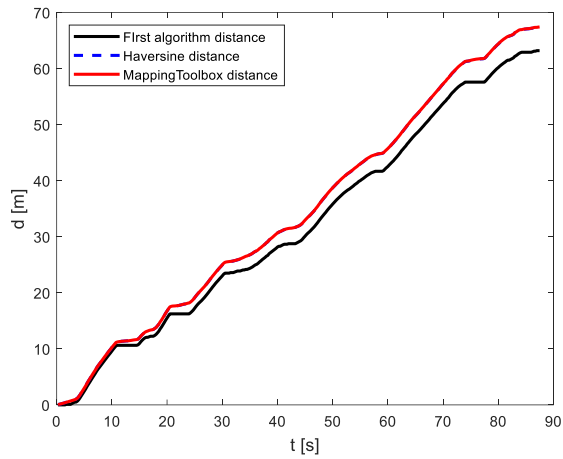


Figure 2.4.5.3 – conf1\_andata\_e\_ritorno\_002.

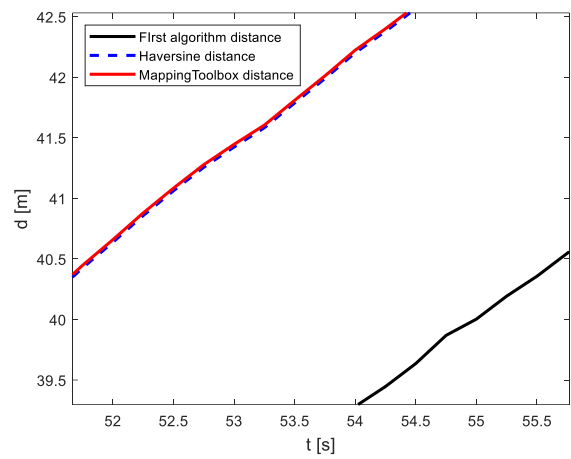


Figure 2.4.5.4 – conf1\_andata\_e\_ritorno\_002.

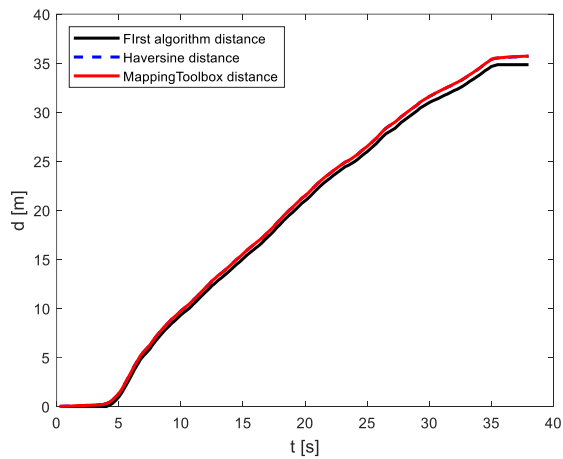


Figure 2.4.5.5 – conf1\_cerchio\_antiorario\_001.

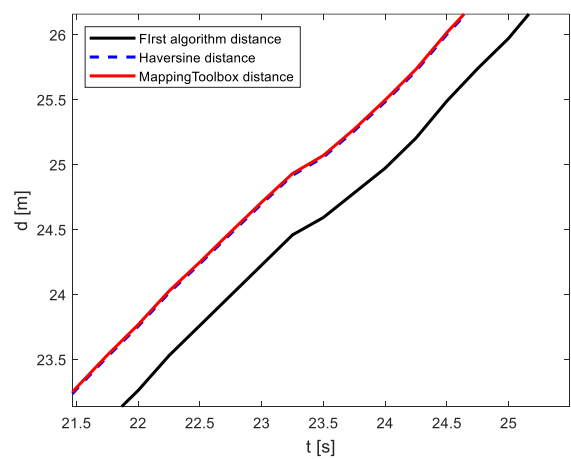


Figure 2.4.5.6 – conf1\_cerchio\_antiorario\_001.

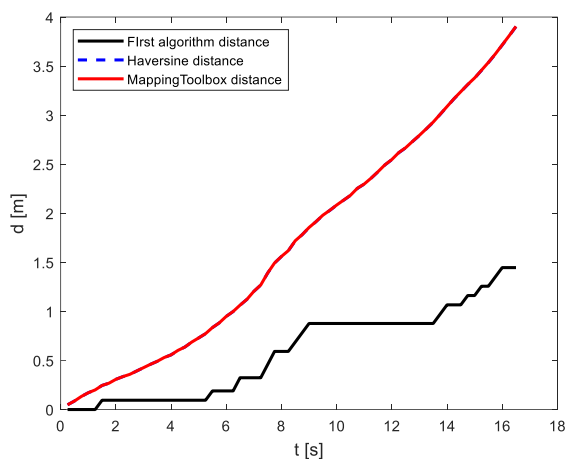


Figure 2.4.5.7 – conf1\_fermo\_001.

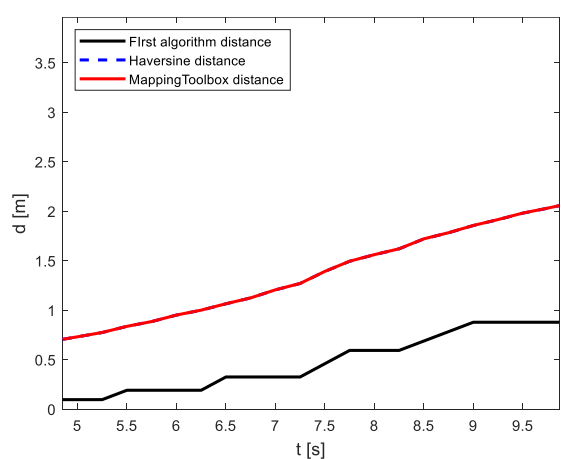


Figure 2.4.5.8 – conf1\_fermo\_001.

The Figure 2.4.5.7 and the Figure 2.4.5.8 shows what could be considered the limit scenario for the differences in the distance calculations, because of the small fictitious vehicle movement determined by the GPS position correction that the Mapping Toolbox code and the Haversine code



are able to use for the distance computation, while the “first algorithm” cannot process in a precise manner. The test “confl\_fermo\_001” is still an interesting case study because accentuate the first algorithm conservative behavior in distance calculation. Considering that the vehicle is still, the first algorithm produces the best results in terms of distance computation. However, this is a limit case, not enough to make the first algorithm preferred on the others.

## 2.5 Velocity data analysis

The velocity data can be obtained in two main ways: the first is to collect the velocities data directly acquired by the GPS receiver; the second concerns the distance data processed with the integration of the time information. Both ways present issues in data understanding, that is why it is mandatory a deeper study on both.

### 2.5.1 GPS velocities data

The GPS receiver used during the tests collects four speed data, or better, three velocity and one speed. The velocities are the North velocity, the East velocity, and the Up velocity, while the speed data is reported as GPS Speed. The main difference between these two classes of information is that the velocities are vectorial quantities being defined by a module and the direction (North, East, Up), while the GPS Speed is a scalar quantity not having the direction datum. It is extremely important now to define in a better way all these quantities and what is the link between them.

If we consider that the velocity assumed by vehicle in each measured time interval can be represented by a 3-D vector, the North velocity will be the projection of the velocity vector on the north direction, i.e., the latitude-changing direction; the East velocity will be the projection of the velocity vector on the east direction, i.e. the longitude-changing direction; the Up velocity will be the projection of the velocity vector on the altitude-moving direction. That means that the GPS receiver gives the speed with which the vehicle it is moving toward the north pole, the speed toward the east, and the speed with which is changing its altitude.

The GPS Speed information it is the module of the velocity vector composed by the sum of the North, the East, and the Up components. This result it is confirmed by comparing the velocity data with a Matlab script. In fact, the module of the vector found combining the North, the East and the Up velocity is comparable with the GPS Speed information. For the test purposes, the Up velocity loose meaning for two main reasons: the first is that the altitude information comes from an interpolation of the latitude and longitude data with a database containing the altitude, so it is a not precise information without the integrated usage of a specific altimeter or barometer; the second reason is that our test will be performed in a constant altitude. The speed needed can be obtained both summing the North and East velocities, intended as vectors, or subtracting the share of the Up velocity from the GPS Speed in the Pythagorean theorem knowing to what vector corresponds the GPS Speed scalar information. In Figure 2.5.1.1 have been plotted the speeds resulting by the summing the vectors of the North and East velocities and the speed resulting by the GPS Speed and Up speed computations from the test “andata\_e\_ritorno\_002”.

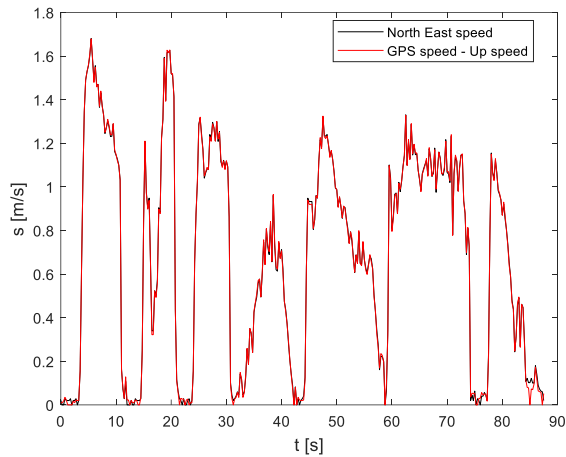


Figure 2.5.1.1 – Speed comparison.

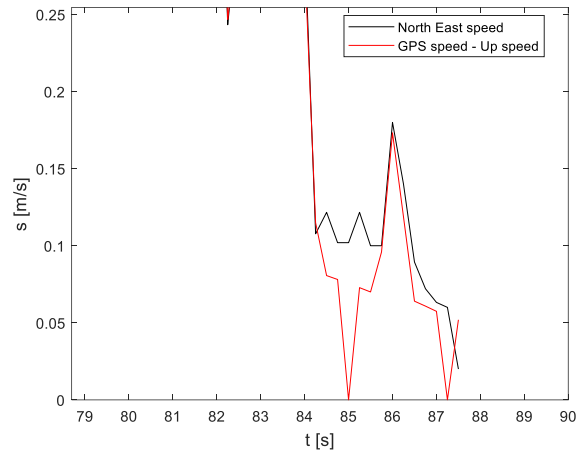


Figure 2.5.1.2– Speed comparison, zoomed view.

The computed speeds lead to the same results, except for module value around the 0,1 m/s where the North East speed tends to assume a constant value of speed instead of showing a null value, as shown in Figure 2.5.1.2.

Among all the velocity information acquired by the GPS receiver, there is not a significant factor that discriminates the choice between the two options, even if the speed computed from the Up and the GPS speed gives more precise values for almost null velocities.

## 2.5.2 Speed computation by latitude-longitude information

Earlier in this report it was described that it is possible to compute the vehicle speed information knowing the coordinates of the vehicle and the sample frequency of the GPS receiver. From the coordinates information it is possible to compute distances between those coordinates, and once knowing the distances travelled in each time step, the average velocity between two spot it is found. Considering that the distance information can be computed following different algorithms, it is interesting to compare the speed information coming from the distances computation and the speed information directly acquired by the GPS. In Figure 2.5.2.1 are shown the results obtained for the test “confl\_andata\_e\_ritorno\_001”, but the results can be extended for all the tests performed.

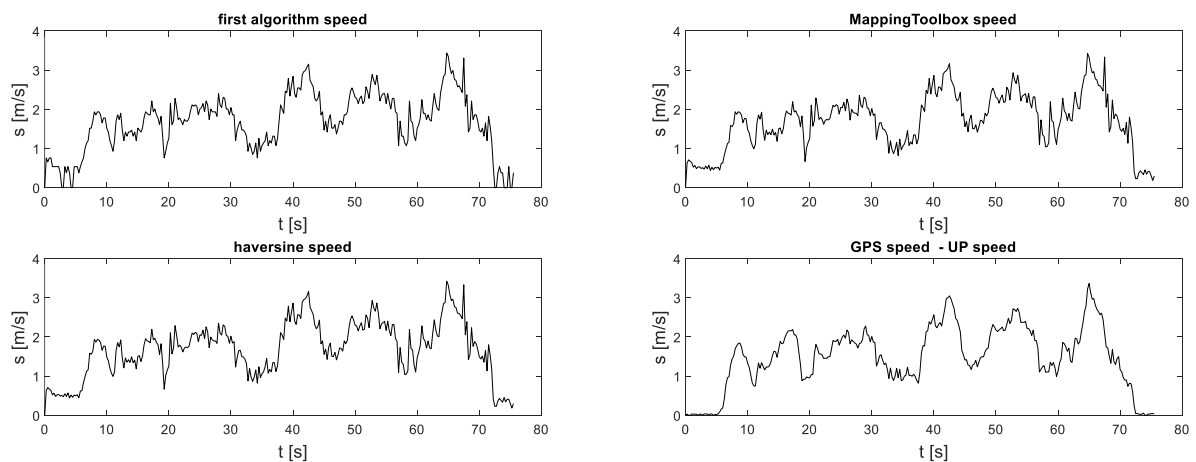


Figure 2.5.2.1 – Comparative of speeds calculated by means of different algorithms and the GPS receiver speed.

Despite existing differences between all the plots, the Matlab Mapping Toolbox and the haversine algorithms give results that have the same behavior and lead to very close results, while the “first algorithm” tends to behave differently when the registered speed is constant cutting these constant speeds to zero. Considering the GPS Speed minus the Up speed as reference, the “first algorithm” approximates better the speeds when the vehicle is stopping, while the Mapping Toolbox and haversine algorithms lead to a better overall speed result.

The speed obtained from the algorithms for distances computation gives results in line with the ones acquired by the GPS receiver, however the computational effort done using the distance algorithms does not pay with a better speed information that results to be more precise in the GPS receiver data. For this reason, it is chosen the GPS receiver speed data to be the right reference, while the speed computation coming from the three distance algorithms will not be used any longer.

## 2.6 Conclusions

In conclusion, different data requires different computational methods.

The distance between two consecutive points is better computed by the Mapping Toolbox algorithm. However, it is important to underline that neither of the three algorithms written produces errors over the 10%, the limit acceptable value.

When the velocity computation is required, the best option to choose is the speed data coming from the GPS receiver. Note that the speed values that better approximate the moving state of the vehicle is not a vectorial quantity, so does not allow a direct understanding of the vehicle direction.

### 3 Wheels steering angle measurement

The aim of this chapter is to find the wheel angle measure, that will be used for the dynamic study of the vehicle. The definition of the vehicle wheel steering angle retrieved from the measure of an easier element displacement is what it is investigated in this chapter. The problem with the wheel steering angle is that is not effortlessly measurable during the vehicle motion due to the element working conditions. Alternative wheel angle measure is investigated after the definition of the vehicle steering system.

#### 3.1 Losi 5ive steering system

The Losi 5ive-T 2.0 uses a series of rods and rotating elements to steer the wheel. It is a relatively easy mechanical system, moved by a servomotor. The whole system is represented in Figure 3.1.1.

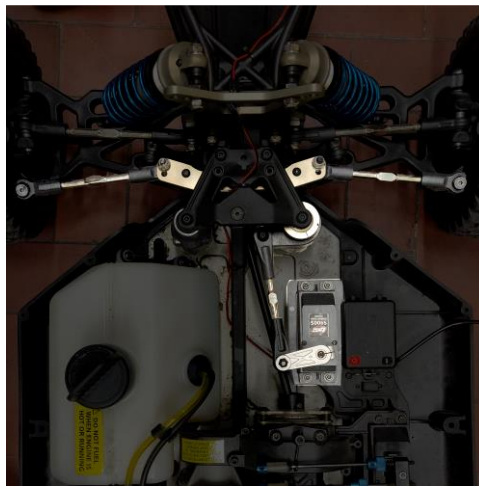


Figure 3.1.1 – Steering system.

Its functioning can be described as follows. The wheel steering is imposed by the movement of two rods that connects the two front wheel with a steering rack.

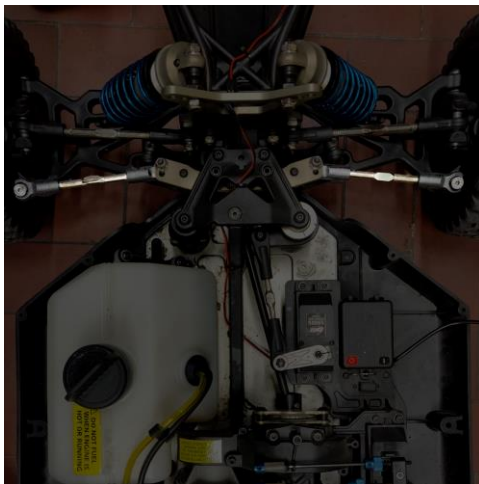


Figure 3.1.2 – Rhods.

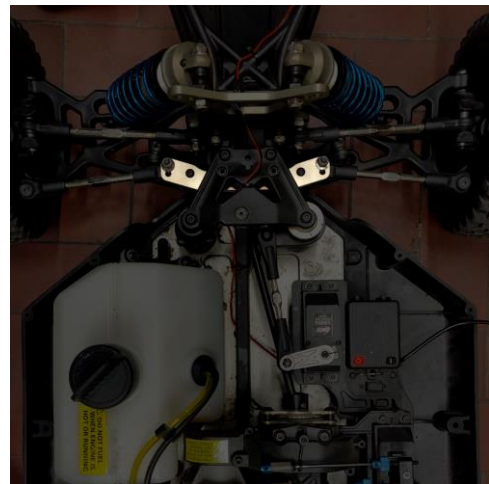


Figure 3.1.3 – Steering rack.

The steering rack is connected to the chassis thanks to two bellcrank that rotate around their axes. The utilization of two bellcrank permits the steering rack to move parallel to the initial position. The right side bellcrank is connected to the steering linkage that is directly moved by the servomotor.

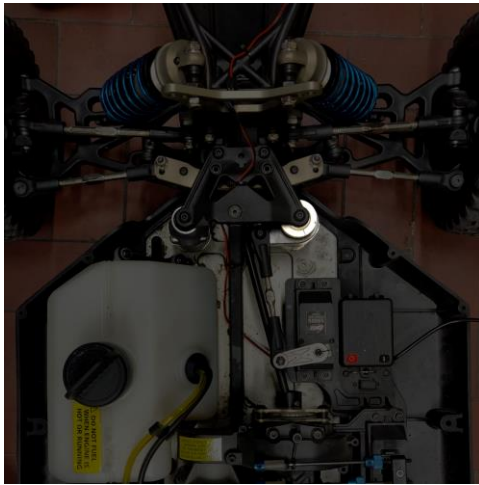


Figure 3.1.4 – Bellcrank.

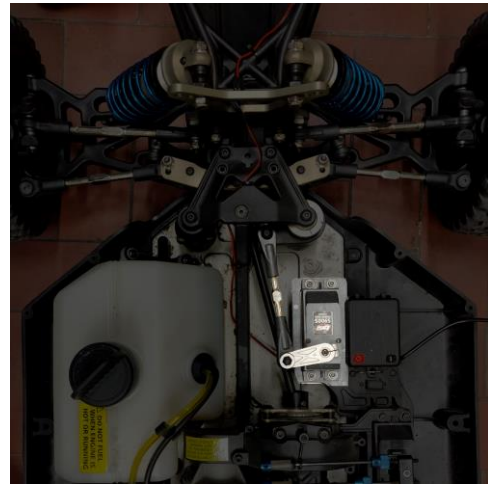


Figure 3.1.5 – Steering linkage and servomotor.

The servomotor receives the activation signal by the radio receiver, commanded by the remote controller.

Understood how the steering system works, to acquire the steering information can be exploited two ways. A first way is to create a derivation system that captures the electric signal the receiver is giving to the servomotor. A second way is measuring the angle of the steering linkage, or the bellcrank, and find a correlation between this angle and the wheel steering angle.

In the next paragraphs are described both the methods.

### 3.2 Wheel angle measure

The final purpose of this chapter is creating a model that allows an easy measure of the wheel steering angle, without the direct measure of that dimension on the wheel. The first step to take before the creation of the model is set a valid reference, created by the direct measure on the vehicle of the wheel steering angle. The measure that will be acquired is a length on a graduated scale. On the graduated scale is projected the wheel relative orientation on respect to the Bosh profile, using a level. The wheel steering angle is obtained using trigonometric relations, knowing the distance between the wheel center and the graduated scale and the length value measure. Then, the obtained wheel steering angle is associated to the servomotor angular displacement. This last step will be used for the next phase, i.e., the steering system model creation.

This measures phase is conducted in the DIMEAS laboratory. The measures are taken using the equipment shown in Figure 3.2.1 and Figure 3.2.2



Figure 3.2.1 – Front view



Figure 3.2.2 – Top view

The equipment consists in a structure built with two Bosh Rexroth aluminum profiles connected by a corner bracket. The Figure 3.2.3 shows the section of the Bosh Rexroth profile, while in Figure 3.2.4 is represented the Bosh Rexroth corner bracket.



Figure 3.2.3 – Bosh Rexroth profile section.



Figure 3.2.4 – Bosh Rexroth corner bracket.

The profiles are secured to the Losi 5ive chassis with two bolts M5x30, as shown in Figure 3.2.5.

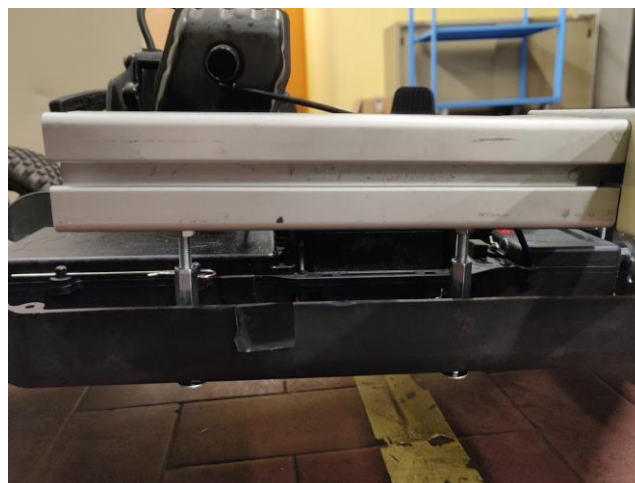


Figure 3.2.5 – Bosh Rexroth profile mount.



A graduated scale is mounted on the profile parallel to the y vehicle's direction, as shown in Figure 3.2.6. The graduated scale is mounted paying attention setting the zero value in correspondence with the wheel zero steering angle.

A second graduated scale is mounted under the servomotor rotating element to link the servomotor angular displacement measure with the wheel steering angle measure.



Figure 3.2.6 – Bosh Rexroth, graduated scale.

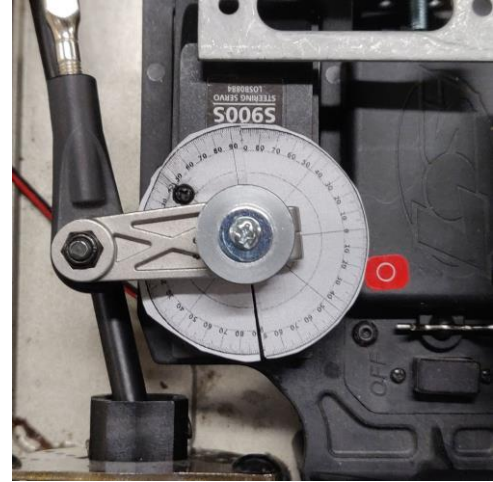


Figure 3.2.7– Servomotor, graduated scale.

The measures taken are reported in the Table 3.2.1. Under the “Servomotor” column are reported the angular displacement in degrees directly measured in the graduated scale, shown in Figure 3.2.7. The “B” column shows the length values read on the graduated scale; the “B” dimension is represented in Figure 3.2.9. In the third column there is the computation results of the wheel steering angle  $\delta$  in degrees, Figure 3.2.9. Since there is a right angle between the A and the B sides of the triangle in Figure 3.2.9, the angle  $\delta$  can be computed with the trigonometric formula:

$$\delta = \arctg(B / A) \quad (3.2.1)$$

With  $A = 155mm$ .

Table 3.2.1 – Wheel angle measures.

Servomotor [deg]	B [mm]	Steering angle [deg]
5	9.0	3.32
	11.0	4.06
10	22.0	8.08
	24.0	8.80
15	28.5	10.42
	30.0	10.95
20	37.0	13.43
	40.0	14.47
25	43.0	15.51
	47.0	16.87
30	59.0	19.54
	55.0	20.84
35	70.0	23.38

	67.0	24.31
41	79.0	27.59
	81.0	27.01

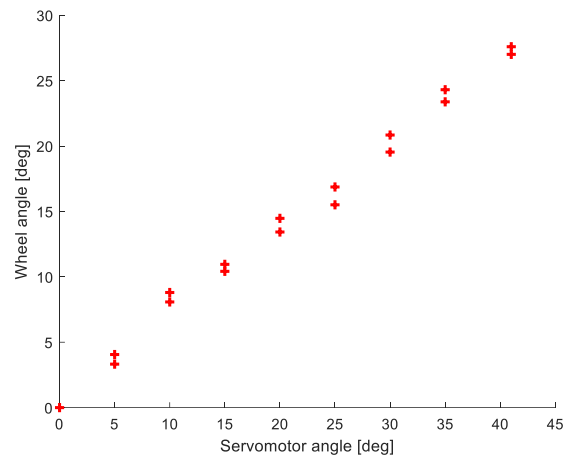


Figure 3.2.8– Correlation between wheel steering angle and servomotor angle.

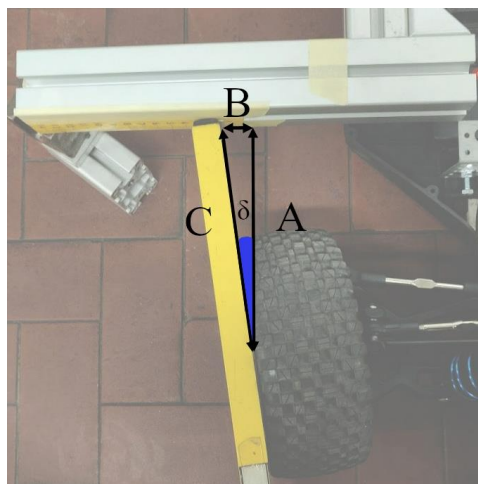


Figure 3.2.9 – Measure triangle.

The steering angle values reported in the Table 3.2.1 and plotted in the Figure 3.2.8 from now on are taken as reference to which compare the models results.

### 3.3 PXI acquisition, direct electric measure of the steering angle

The base idea of this first steering angle acquiring method, is to intercept and store the command signal the radio receiver is transferring to the servomotor. The signal is sampled with a NI PXI (Figure 3.3.1) and processed in Matlab to retrieve the wheel steering angle. NI PXI systems provide high-performance modular instruments and other I/O modules that feature specialized synchronization and key software features for test and measurement applications from device validation to automated production test [7].





Figure 3.3.1 – NI PXI System.

The first step to take is analyzing the Losi 5ive-T 2.0 radio receiver, a Spektrum SR6000T receiver, shown in Figure 3.3.2.



Figure 3.3.2 – Spektrum SR6000T receiver.

The receiver has various input/output ports. The ports that are collocated in the left side of the Figure 3.3.2 are composed by three pin: the “+”, the “-“, and the “S”. The first two pins are related to the alimentation of the elements connecting to the receiver, while the “S” is the pin assigned for the signal transmission. The ports are: the battery input “BAT”, the steering port to which the servomotor will be connected “STR”, the throttle “THR”, and four auxiliary ports utilized for the connection of accessories. In the examined Losi 5ive the “AUX1” port is utilized for the front lights’ alimentation. The right-side ports represented in the Figure 3.3.2, could be generically identified as “bus ports” and are intended to be used with specific accessories. In particular, the “RPM” port allows to connect of a RPM sensor, the “TEMP” allows the introduction of a temperature sensor, the “VOLT” allows the utilization of a voltmeter and the “XBUS” port is a generic bus port. Note that these extra sensors are compatible only with an electric engine; the Losi 5ive-T 2.0 has a 32cc gasoline engine, so these sensors cannot be used.

### 3.3.1 PXI acquisition tests

The port that it is interesting for the steering study is the “STR”. From this port the receiver sends a signal to the servomotor. With the acquisition of this signal could be possible to retrieve the wheel steering angle implementing a Matlab code. The signal is intercepted connecting to the receiver

“STR” port a plug with two outputs, one dedicated to a NI PXI System and one to the servomotor. The connection with the NI PXI is made using a NI SCB-68A (Figure 3.3.1.1), a 68-Pin shielded connector block. The NI SCB-68A provides 68 screw terminals that can be used as input/output connection. The available connections are reported in the connection block cover (Figure 3.3.1.2).

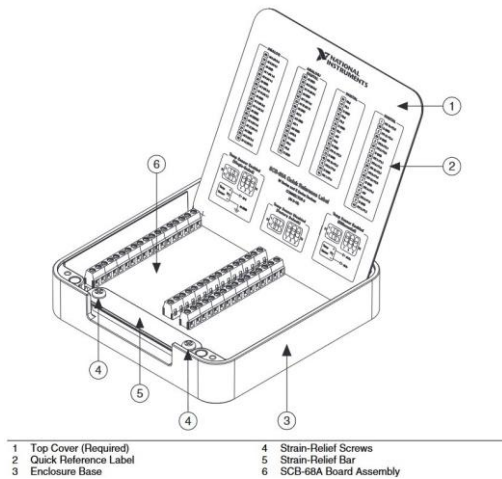


Figure 3.3.1.1– NI SCB-68A.



Figure 3.3.1.2– NI SCB-68A, cover.

Figure 3.3.1.3 shows how the plug is connected to the receiver while Figure 3.3.1.4 shows the connection between the receiver and the NI connector block.

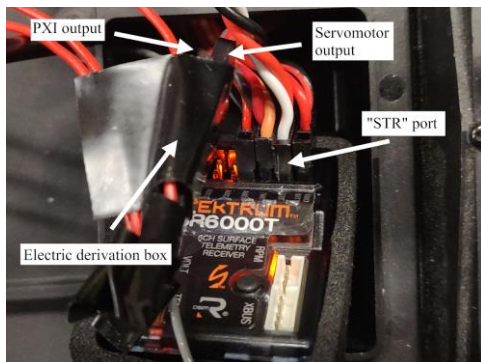


Figure 3.3.1.3 – Plug connection.

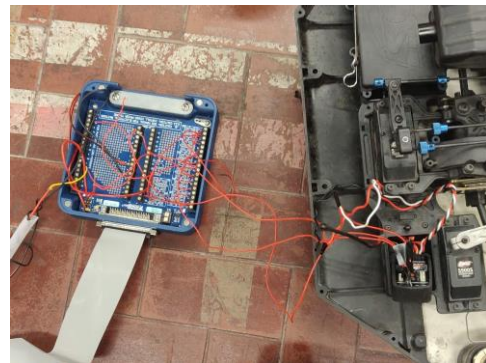


Figure 3.3.1.4– PXI connection.

The signal is acquired imposing six different configurations to the steering system, in particular: ten seconds, no steering; ten seconds, left steering; ten seconds, right steering; five seconds for each no steering-left steering-no steering-right steering-no steering; continuously changing steering direction; ten seconds acquisition with throttle at maximum, ten seconds acquisition with throttle at minimum (braking). The NI software allows the exportation of the test data in a “.csv” file. This file is imported and processed in Matlab. The results obtained are plotted in the following figures.

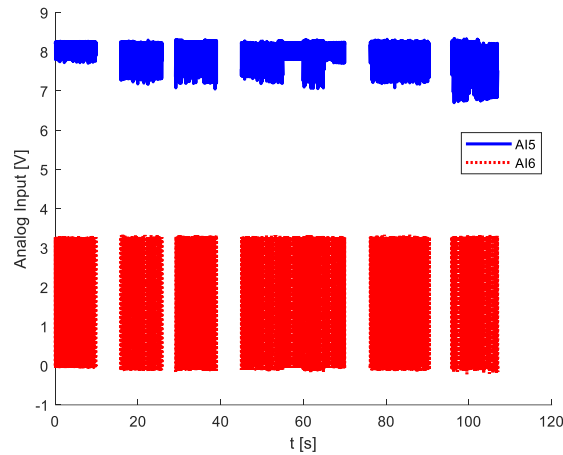


Figure 3.3.1.5 – Total view of the data acquired.

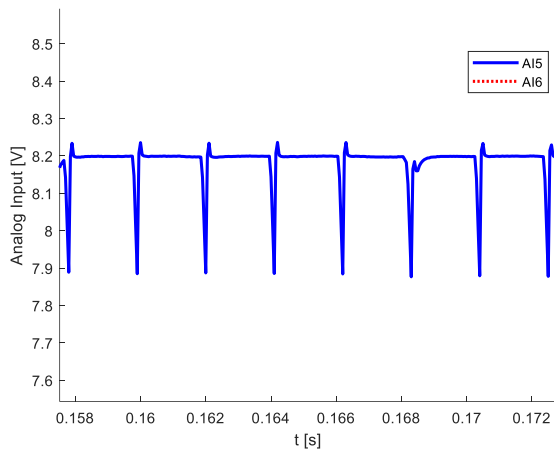


Figure 3.3.1.6 – AI 5.

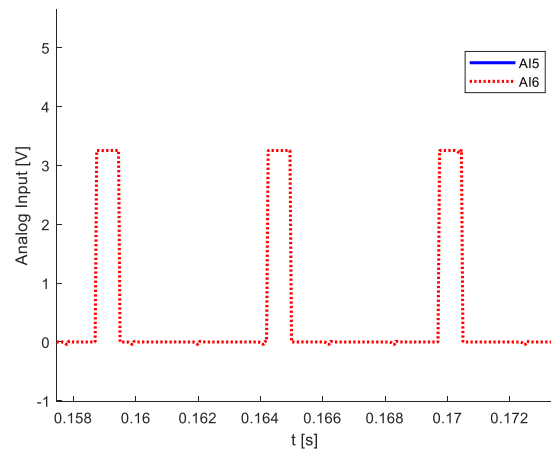


Figure 3.3.1.7– AI 6.

The signals found are digital signals. Without knowing the signal codification logic, it is impossible to establish the meaning of the signal acquired, i.e., it is impossible to retrieve the steering angle from these data. If analog signals were found, the post-process phase could have been conducted. The steering information needed can be obtained in different ways that will be exploited in the following paragraphs.

### 3.4 Steering system CAD models

The wheel steering angle can be derived by the study of the Losi 5ive-T 2.0 steering system. The main goal of this paragraph is to find a model that can give the wheel steering angle knowing as input the servomotor angle displacement. Once a model is validated, the servomotor angle displacement acquisition will be performed using a potentiometer, that associates an output voltage to a servomotor angle displacement.

#### 3.4.1 Matlab model

The first investigated method is performed building a mathematical model that provides a direct link between the servomotor rotational displacement and the wheel steering angle. A set of equations have been written starting from the kinematic study of the steering system.

The kinematic study has been performed dividing the steering system into two subsystems. The first subsystem consists of servomotor, servomotor rod and bellcrank, already shown in the Figure 3.1.4 and Figure 3.1.5. The second subsystem consists of the second arm of the bellcrank, the steering rack and the wheel rod. The system has been schematized as represented in Figure 3.4.1.1.

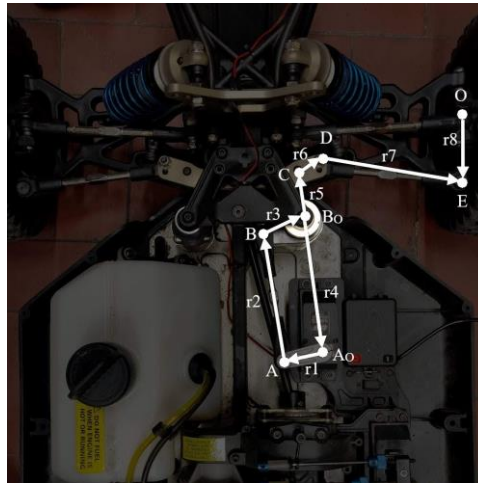


Figure 3.4.1.1 – System scheme.

The first subsystem is studied as an articulated quadrilateral (Figure 3.4.1.2), considering the  $r_1$  as the servomotor rotating part, the  $r_2$  the servomotor rod and the  $r_3$  the first of the two bellcrank arms.

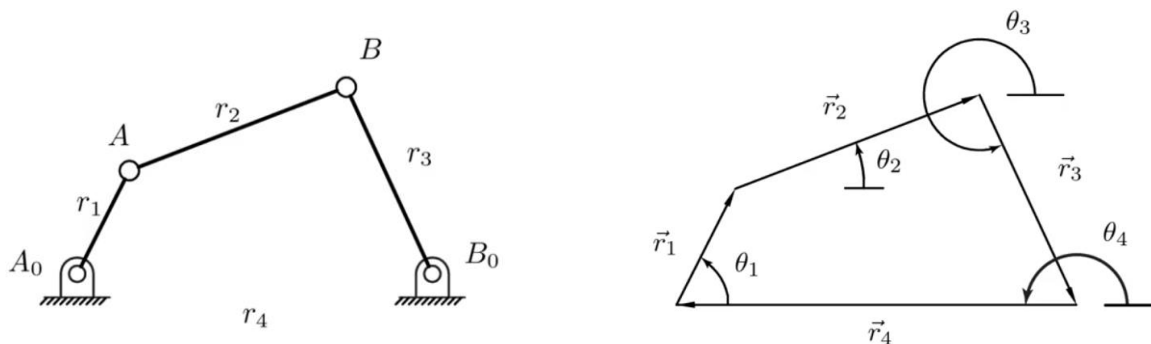


Figure 3.4.1.2 – Articulated quadrilateral.

The kinematic of the quadrilateral joints are studied introducing the vectorial position components. Each of the joints can be identified by a vector  $r$  and an angle. The angles are measured considering positive the rotation increment in the anticlockwise orientation of the vectors  $r_i$ . The problem data are the radii  $r_1$ ,  $r_2$ ,  $r_3$ ,  $r_4$  and the angle  $\theta_4$ . The angle  $\theta_1$  is the input from which compute the angles  $\theta_2$  and  $\theta_3$ , that are the unknowns of the problem. In the Table 3.4.1 are reported the data values.

Table 3.4.1.1 – Data.

Dimension	Value
-----------	-------

$r_1$ [mm]	30
$r_2$ [mm]	100
$r_3$ [mm]	30.5
$r_4$ [mm]	105.03
$\theta_4$ [rad]	$\pi$

The kinematic solutions are found using the loop closure equation method, eq. (3.4.1.1).

$$\bar{r}_1 + \bar{r}_2 + \bar{r}_3 + \bar{r}_4 = 0 \quad (3.4.1.1)$$

The eq. (3.4.1.1) has been written introducing the complex notation and then, using the Euler's formula, the real part and the imaginary part of the equation has been studied separately eqs. (3.4.1.2).

$$\begin{cases} r_1 \cos \theta_1 + r_2 \cos \theta_2 + r_3 \cos \theta_3 + r_4 \cos \theta_4 = 0 \\ i(r_1 \sin \theta_1 + r_2 \sin \theta_2 + r_3 \sin \theta_3 + r_4 \sin \theta_4) = 0 \end{cases} \quad (3.4.1.2)$$

Powering to two the equation of the system eqs. (3.4.1.2), then summing the two equations, remembering that the angle  $\theta_4$  is equal to  $\pi$ , and introducing further algebraic manipulations, the following system is found eqs. (3.4.1.3).

$$\begin{cases} A \sin \theta_3 + B \sin \theta_3 + C = 0 \\ A = r_1^2 - r_2^2 + (r_3 + r_4)^2 - 2r_1 \cos \theta_1 (r_3 + r_4) \\ B = 4r_1 r_3 \sin \theta_1 \\ C = r_1^2 - r_2^2 + (r_3 - r_4)^2 - 2r_1 \cos \theta_1 (r_3 - r_4) \end{cases} \quad (3.4.1.3)$$

One possible strategy for the solution of the system is introducing the trigonometric identities shown in eq. (3.4.1.4).

$$\begin{cases} \operatorname{tg} \left( \frac{\theta_3}{2} \right) = t \\ \sin \theta_3 = \frac{2t}{1+t^2} \\ \cos \theta_3 = \frac{1-t^2}{1+t^2} \end{cases} \quad (3.4.1.4)$$

With this strategy, the first equation of the eq. (3.4.1.3) becomes second order equation eq. (3.4.1.5).

$$(B - C)t^2 + 2At + B + C = 0 \quad (3.4.1.5)$$

The equation eq. (3.4.1.5) could have no real solution, two coincident solution or two distinct real solution, based on the value of the equation discriminant  $\Delta$ . If the equation have two real roots  $t_1$  and  $t_2$ , two values of  $\theta_3$  are found, as follows from (eq. (3.4.1.6)).

$$\begin{cases} \theta_3' = 2 \arctg(t_1) \\ \theta_3'' = 2 \arctg(t_2) \end{cases} \quad (3.4.1.6)$$

It is now possible to compute the  $\theta_2$  angle from the eq. (3.4.1.2). The one  $\theta_3$  angle, and the corresponding  $\theta_2$ , that must be taken depends on the initial condition of the system. Once represented the joint positions for both the solutions, the right one can be picked. From the first subsystem results it is possible to compute the position of the points A and B with the following equations:

$$\begin{cases} x_A = r_1 \cos \theta_1 \\ y_A = r_1 \sin \theta_1 \end{cases} \quad \begin{cases} x_B = r_1 \cos \theta_1 + r_2 \cos \theta_2 \\ y_B = r_1 \sin \theta_1 + r_2 \sin \theta_2 \end{cases} \quad (3.4.1.7)$$

Once obtained the  $\theta_3$  angle, it is possible to continue the study of the second steering subsystem. The  $\theta_3$  represents the rotation of the bellcrank; from this rotation are computed the values of the steering rack displacement, the wheel rod displacement, and finally the wheel steering angle. The wheel steering angle comes from the solution of the following equation systems

$$\begin{cases} x_C = r_4 + r_5 \cos \theta_5 \\ y_C = r_5 \sin \theta_5 \\ \theta_5 = \theta_{5,0} - \theta_3 \end{cases} \quad \begin{cases} x_D = x_C + r_6 \cos \theta_{6,0} \\ y_D = y_C + r_6 \sin \theta_{6,0} \end{cases} \quad \begin{cases} x_E = x_D - r_7 \cos(\theta_7 + \theta_{7,0}) \\ y_E = y_D - r_7 \sin(\theta_7 + \theta_{7,0}) \end{cases} \quad (3.4.1.8)$$

Knowing the position of the instantaneous center rotation of the point E, namely the point O, it is possible to retrieve the wheel steering angle as:

$$\theta_8 = \theta_{8,0} + \arctan \frac{x_E - x_O}{y_E - y_O} \quad (3.4.1.9)$$

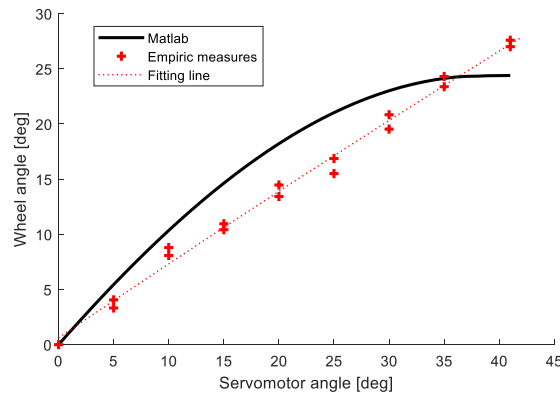


Figure 3.4.1.3 – Matlab results.

As shown in Figure 3.4.1.3, the results obtained with the Matlab code are not good enough to consider this method valid, in fact the maximum difference computed between the Matlab results

and the test measure is around 34%. Other methods should be considered for the retrieve of the wheel steering angle having the servomotor angle measure.

### 3.4.2 Adams View model

MSC ADAMS (Automated Dynamic Analysis of Mechanical Systems) is a multibody dynamics simulation software system. The strength of this software consists in the possibility to retrieve an early system-level design validation without performing a full finite element analysis. MSC ADAMS allows to evaluate and manage “the complex interactions between disciplines including motion, structures, actuation, and controls to better optimize product designs for performance” [8]. The advantage in creating an ADAMS View model is clear: the kinematic study of the steering system does not need to be written in an explicit form anymore. The results can be obtained with the simulation of the ADAMS View model, that, however, must be built accurately. The difficult part is the model construction and the right set up of all the system property, such as geometrical property, connection between elements, motion to impose.

The first step in the model creation consisted in the measure of the steering system elements dimension. All the elements measured are described in paragraph 3.1. Only the fundamental dimensions have been collected for the replication of the ADAMS View model. The aim to recreate a reality-like functioning model, the esthetical aspect played a marginal role. That is the reason why the 3D modeled steering systems elements have a shape slightly different from the original parts. The steering system components and the final assembly have been modelled in SolidWorks. In the following figures are plotted the real parts beside the CAD model.

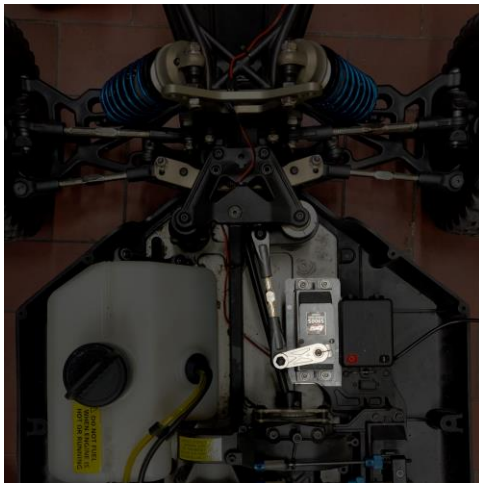


Figure 3.4.2.1 – Servomotor and Rod.

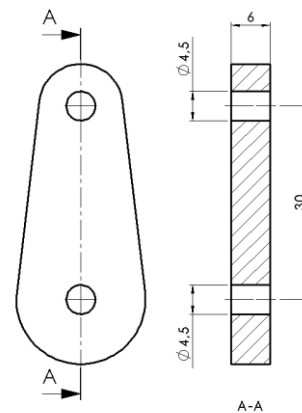


Figure 3.4.2.2 – Servomotor rotating element.



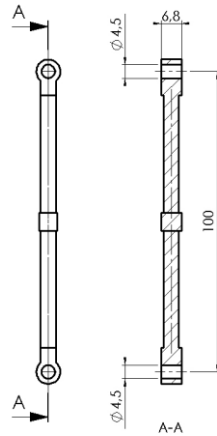


Figure 3.4.2.3 – Servomotor Rod.

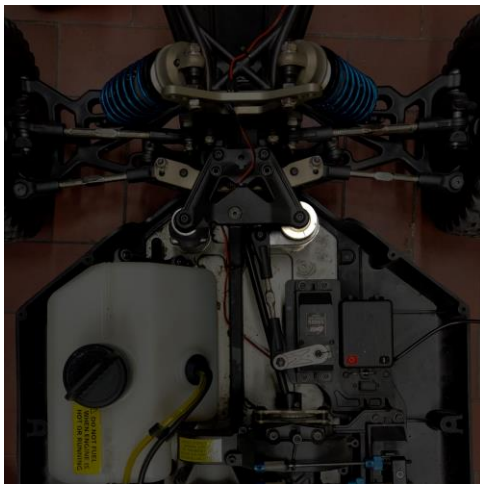


Figure 3.4.2.4 – Bellcrank.

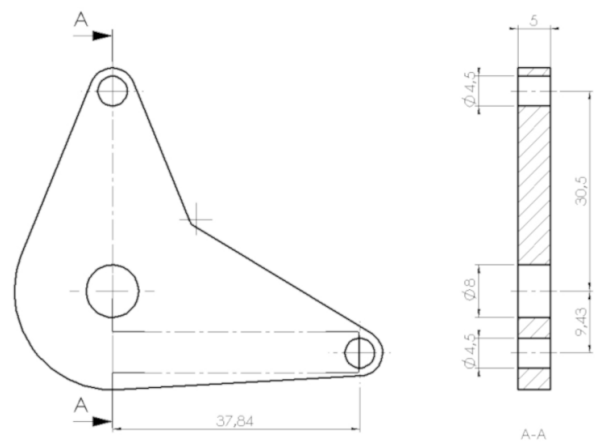


Figure 3.4.2.5 – Bellcrank CAD.

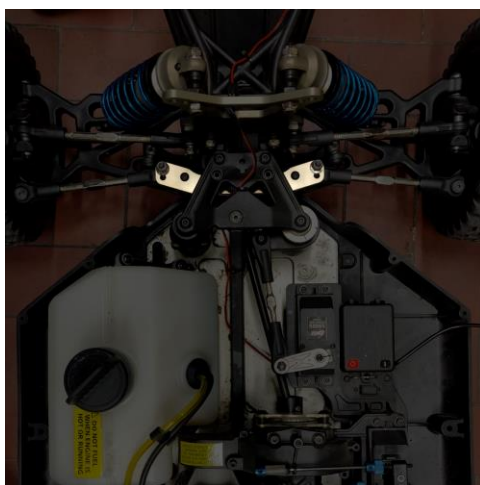


Figure 3.4.2.6 – Steering rack.

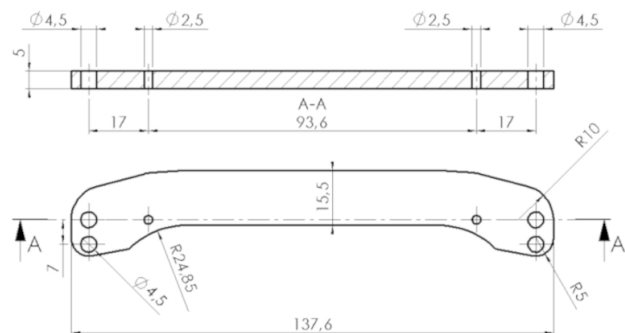


Figure 3.4.2.7 – Steering rack CAD.



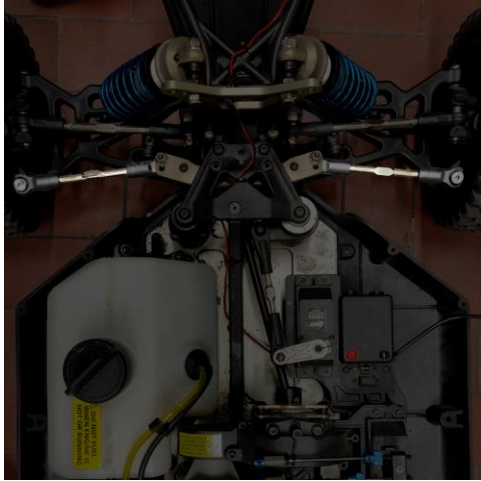


Figure 3.4.2.8 – Wheel rods.

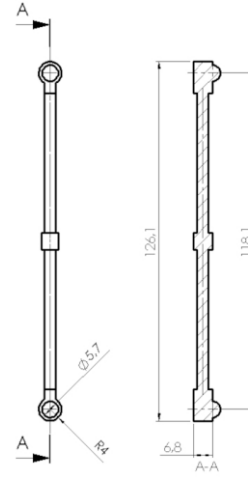


Figure 3.4.2.9 – Wheel rod CAD.

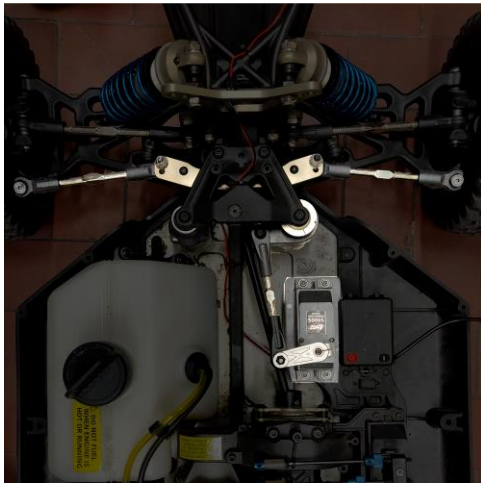


Figure 3.4.2.10 – Steering system.

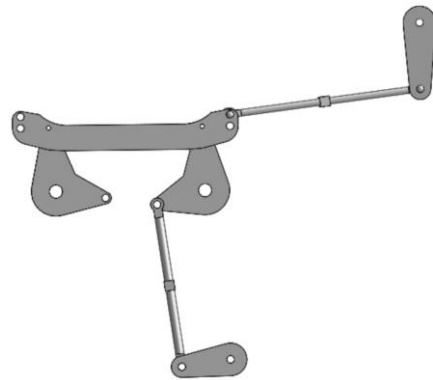


Figure 3.4.2.11 – Steering system 3D CAD.

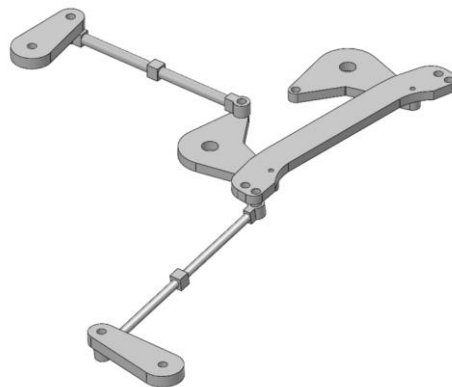


Figure 3.4.2.12 – Steering system 3D CAD, isometric view.

The wheel has been simulated with a component having the dimension corresponding to the distance between the wheel rod terminal part and the instantaneous rotation center around which the rod terminal rotates. The distance is reported in Figure 3.4.1.1 as  $r_8$ .

The full assembly is the exported as a Parasolid “.x\_t” file and imported in ADAMS View. SolidWorks has been preferred in the 3D CAD creation over the ADAMS View 3D design tools for pragmatical reasons. In ADAMS View have been defined the connections between the assembly parts and the motion of the system. In Figure 3.4.2.13 is represented the assembly’s top view, with the connections numbered. In the Table 3.4.2.1 the connections property is reported.

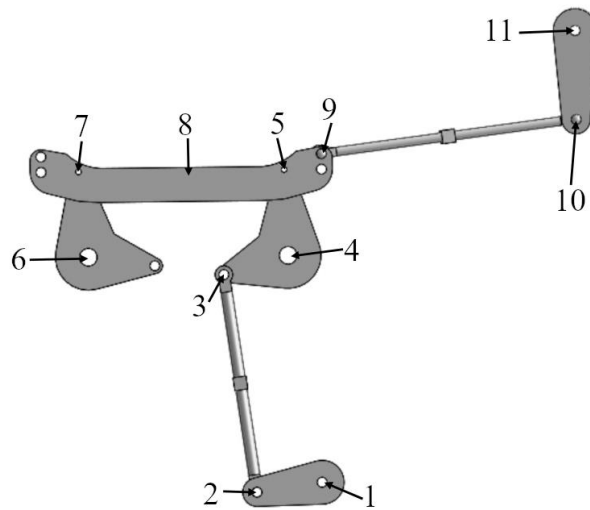


Figure 3.4.2.13 – Steering system 3D CAD, numbered joints.

Table 3.4.2.1 – Steering system joints.

Joint	First body	Second body	Type
1	Ground	Servomotor	Revolute
2	Servomotor	Servomotor rod	Revolute
3	Servomotor rod	Bellcrank	Revolute
4	Ground	Bellcrank	Revolute
5	Bellcrank	Steering rack	Revolute
6	Ground	Bellcrank	Revolute
7	Bellcrank	Steering rack	Revolute
8	Ground	Steering rack	Planar
9	Steering rack	Wheel rod	Revolute
10	Wheel rod	Wheel	Revolute
11	Ground	Wheel	Revolute

The revolute joint allows the relative rotation of two bodies around a specific axis. For the set-up of this joint the body selection order is not relevant for the joint functioning; the rotational axis is identified by the “location” selection in ADAMS View. All the revolute joints are set up using the construction “2 Bodies – 1 Location” “Normal To Grid”.

The planar joint allows to a rigid body plane to rotate and slide on a second rigid body plane. Again, the construction options “2 Bodies – 1 Location” “Normal To Grid” have been used. It is requested the selection of the joint vector during the definition of the planar joint. This vector identifies the joint’s plane of motion. The body that must be fixed in space, if there is one, must be picked as the first body; the second body will rotate and slide in respect to the first one. The planar joint has been

used for the steering rack to make sure this element rotates and slides parallel to the ground, pushed by the bellcrank.

After the definition of the system joints, the rotational motion is imposed to the Joint\_1 and two measures are collected: one on the servomotor moving part (Joint\_1); the second one on the wheel (Joint\_11).

The measure results are plotted in Figure 3.4.2.14.

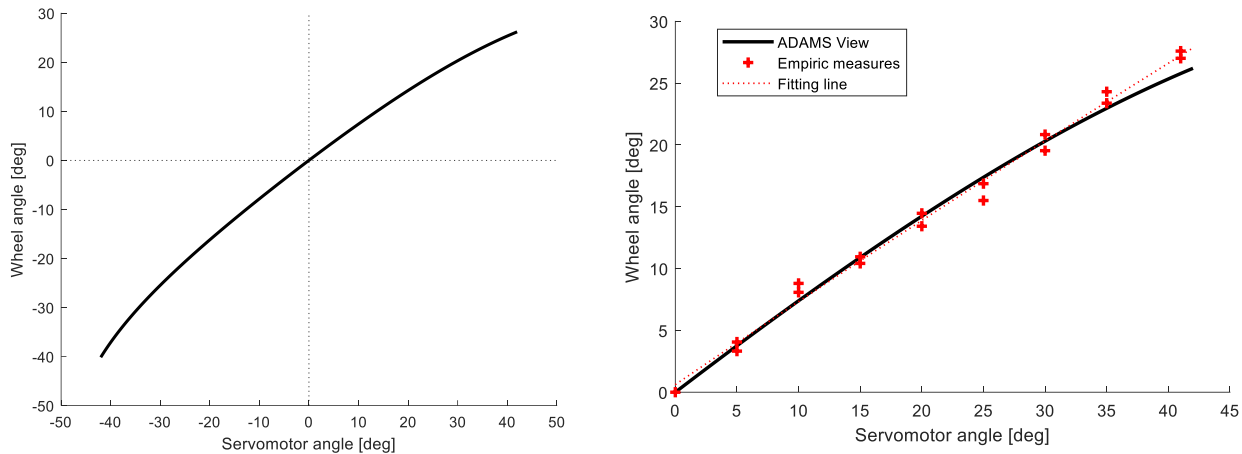


Figure 3.4.2.14 – Left figure: Adams Views results in the correlation between the servomotor angle displacement and the wheel steering angle.

Right figure: Adams View results compared with the empiric measures.

In the right graph of the Figure 3.4.2.14 are plotted the ADAMS View results and the measures acquired as described in the paragraph 3.2. The graph is only reported for positive values of the servomotor angle because the measures could only be acquired for the left vehicle steering, to which corresponds a positive servomotor angle. The fitting line in the right-side plot of the Figure 3.4.2.14 is obtained with the “*polyLMS*” function.

The results show that the ADAMS View model gives a good approximation of the real wheel angle, with a deviance for high steering angle. The error cannot be directly computed from the data coming from the ADAMS View simulation and the measure because of the different input, namely the servomotor angle, used for the wheel steering angle measure. The following solution is utilized for the error computation: starting from the empiric measures, it has been possible to retrieve the polynomial fitting function coefficients thanks to the “*polyLMS*” function. From these coefficients it has been possible to declare a function in Matlab that has the aim to simulate the possible measure that would be collected if was considered as the input the value of the servomotor steering angle coming from the ADAMS simulation. Using this expedient, it is computed the error that exists between the empiric measures and the ADAMS View results. The error has an average value of 2%, with a lower computed error of 0,01%, and the highest computed error of 5,9%. Those results are inside the acceptability validation range and can be used for the wheel steering angle computation with a good level of confidence.

### 3.5 Servomotor angle measure using a potentiometer

As already discussed, the measure of the wheel steering angle could be avoided considering measuring other quantities directly linked with the wheel steering angle. In this chapter is investigated the measure of the servomotor angle displacement.

The servomotor angle displacement is measured with the system shown in Figure 3.5.1 and Figure 3.5.2.

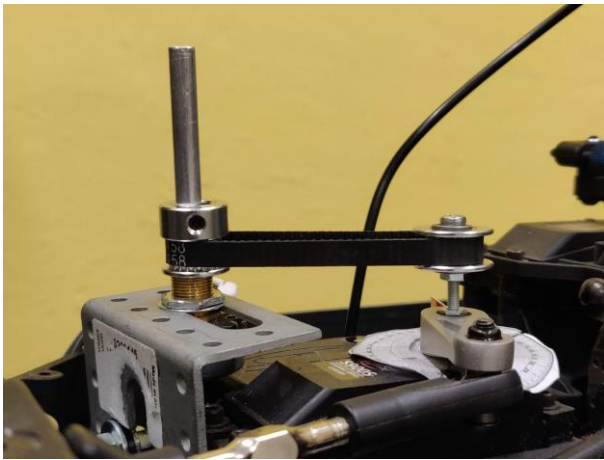


Figure 3.5.1 –Measuring system.

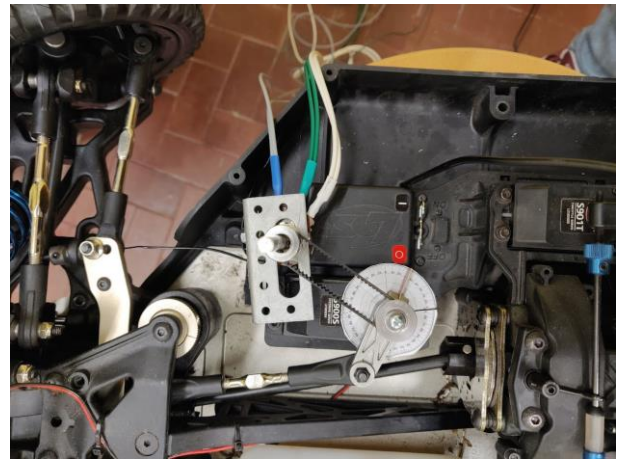


Figure 3.5.2 – Measuring system, top view.

This system is built as follows. The servomotor original screw that connects the electric motor to the rotating part has been substituted by a longer screw M3x30. This new screw has the aim to connect the rotating mechanism to the electric motor and transfer the electric motor rotation to a gear (Figure 3.5.3), secured to the screw with two bolts.



Figure 3.5.3 – Gear.



Figure 3.5.4 – Toothed belt.

The rotating motion is then transferred from the gear to a potentiometer using a toothed belt (Figure 3.5.4) and a second gear mounted on the potentiometer shaft. (Figure 3.5.5). The potentiometer utilized is represented in Figure 3.5.6.



Figure 3.5.5 – Potentiometer gear.



Figure 3.5.6 – Potentiometer.

The potentiometer has been powered with a Dynamite Reaction battery, a 4000mAh, 7.4 Volt lithium polymer battery, shown in Figure 3.5.7. The tension signals measures are acquired using two SCADAS XS analog input. A first analog input has been used to acquire the tension signal  $V_2$  directly coming from the battery, the other analog input has been used to acquire the potential difference  $V_1$  existing from the signal potentiometer port and the negative pole. A simplified circuit scheme for the signal measures is represented in Figure 3.5.8. The battery tension must be considered because of the potential difference lowering caused by the battery drain. If it is not considered this tension lowering, a fictitious steering angle caused by the battery drain and not due to the potential differential variation imposed by the potentiometer would be computed.



Figure 3.5.7 – Li-Po Battery.

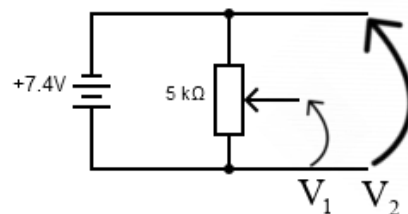


Figure 3.5.8 – Potentiometer measures.

Before connecting the system to the battery, a connection verification has been made with a multimeter. Once the system is ready, it is mandatory to perform three tension measures before the beginning of the steering test itself. These three tensions are needed to give a reference to the subsequent measures. The reference tension system is composed by the no steering condition potential difference  $V_0$ , the minimum potential difference  $V_{min}$  that corresponds to the right-side

steering, and a maximum potential difference  $V_{max}$  that corresponds to the left steering. Note that this reference is valid for the test configuration, measuring the potentiometer signal using the negative pole as reference.

Once the tension to take as reference has been acquired, the battery drain effect must be taken into order. The battery drain over time lowers the potentiometer supply voltage and changes the potential differences reference. The problem can be solved introducing the tension ratio  $p$  computed as the ratio of the  $V_0$ ,  $V_{min}$  or  $V_{max}$  and the instantaneous battery potential difference  $V$  at the time  $t$ .

$$p_i = \frac{V_i}{V_{battery}} \quad (3.5.1)$$

With  $p_i$  that will be  $p_{max}$ ,  $p_{min}$  or  $p_0$  if computed respectively using  $V_0$ ,  $V_{min}$  or  $V_{max}$ . gg

The tension system will be no longer based directly on the tensions  $V_0$ ,  $V_{min}$  and  $V_{max}$ , meaning that the system reference will be time invariant. It is now possible to identify the relationship between the measured tension signal  $V_1$  and the servomotor rotation displacement knowing the maximum and the minimum rotation that the servomotor could perform.

The correlation between potential difference ratio and servomotor angle displacement it is found writing a Matlab code. This code creates a datasheet with two columns, the first one containing the potential ratio, and the second one the corresponding servomotor angle. Using the Matlab code it is possible to enter a potential value, the corresponding instantaneous battery voltage, and the reference tensions, and retrieve the corresponding servomotor angular displacement. In Figure 3.5.9 it is plotted the servomotor angle - differential potential ratio correlation graph. If the signal had been measured using the positive pole of the battery as reference, the graph would have shown a curve with a decreasing trend instead of an increasing trend as happens in Figure 3.5.9. The decreasing trend is justified by the fact that the  $V_{max}$  would be associated to a left steering instead of the right steering, and the  $V_{min}$  would be associated to the right steering.

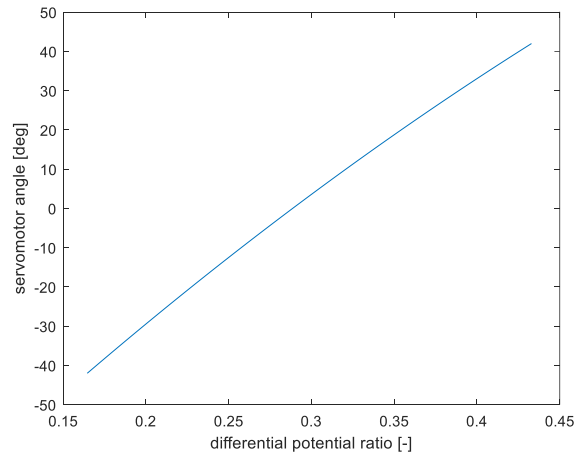


Figure 3.5.9 – Servomotor angle function of differential potential ratio.

### 3.6 Wheel angle estimation using the potentiometer data

In the previous paragraph have been found the correlation between the servomotor angular displacement and the wheel steering angle, and the correlation between the potentiometer tension signal and the servomotor angular displacement. The two built model have the final aim to evaluate the wheel steering angle starting from an analog tension signal.

In Figure 3.6.1 is represented the results coming from the Matlab code that correlates the potentiometer voltage signal to the wheel steering angle. The Test 11 of 15 performed with the IMU and the potentiometer acquisition has been taken as example. The test with the IMU will be discussed later in the thesis. The plotted graph has on the y-axis the wheel steering angle and on the x-axis the potentiometer. What is expected is the wheel steering angle values should go from -25 degrees to 25 degrees, while the potentiometer signal value depends on the battery discharge during the test and on the rotation of the potentiometer shaft. The possible potentiometer values can change in a range that goes from 0 Volt to around 7.9 Volt, that is the average battery voltage measured during the tests. Ideally the voltage tension should not take values about equal to the limits, due to the potentiometers properties, making a good variation range the 1.5 Volt till 6 Volt.

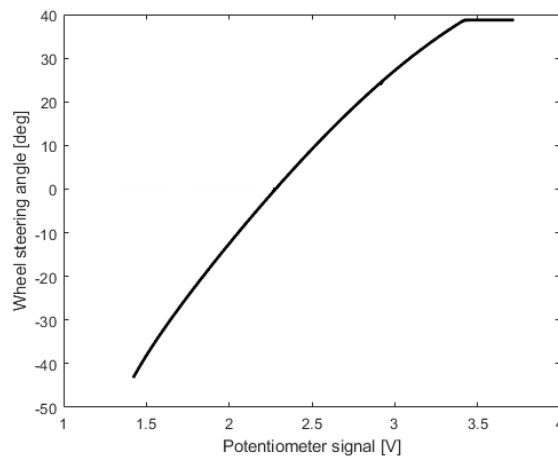


Fig Figure 3.6.1 – Potentiometer – Wheel angle.

In the Figure 3.6.1 is reported the curve wheel steering angle function of the potentiometer signal. The tension range utilized is good and should not interfere with the servomotor angle measures. The  $V_0$ ,  $V_{min}$  or  $V_{max}$  discussed in the paragraph 3.5 in this case could be identified respectively as 2.4 V, 1.4 V and 3.4 V. The Figure 3.6.2 shows the comparison between the results of two consecutive test, chosen to minimize the battery drain effects on the curve shifting.

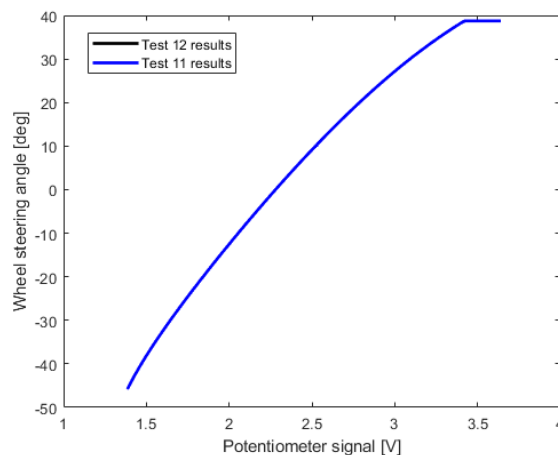


Figure 3.6.2 – Test 11 results compared to Test 12 results.

A more in deep focus should be considered. The main issue is that the computed wheel steering angle should not assume values out of the -25 to 25 degrees. The potentiometer has been installed

paying attention that the shaft rotation was far from the mechanical rotation limits of the sensor, therefore there should not be criticism about the mechanical assembly. The possible causes of this wrong results could be investigated on the Matlab code possible errors for the process of high clusters of data. If a single voltage measure is given to the code, it is possible to retrieve the wheel angle data with a good level of precision. The difficulties of the high clusters of data consist in the resolution of the bellcrank rotation equation by Matlab that, for vectors containing  $10^6$  values, would take a serious amount of time for the results computation and possibly lead to calculation errors.



## 4 Vehicle Dynamics

The vehicle dynamic study is performed with the utilization of a set of accelerometers and thanks to an IMU. After a rapid introduction to the vehicle dynamics, the experimental tests are described.

### 4.1 Bicycle model.

A rapid description of the single-track model is now discussed for a better understanding of the experiment performed in the following paragraphs. The bicycle model, or single track model, is a simplified car model. Despite the strong simplification brought, this model allows an approximate, but still plausible, vehicle dynamic description. In Figure 4.1.1 there is a graphic representation of the model [9].

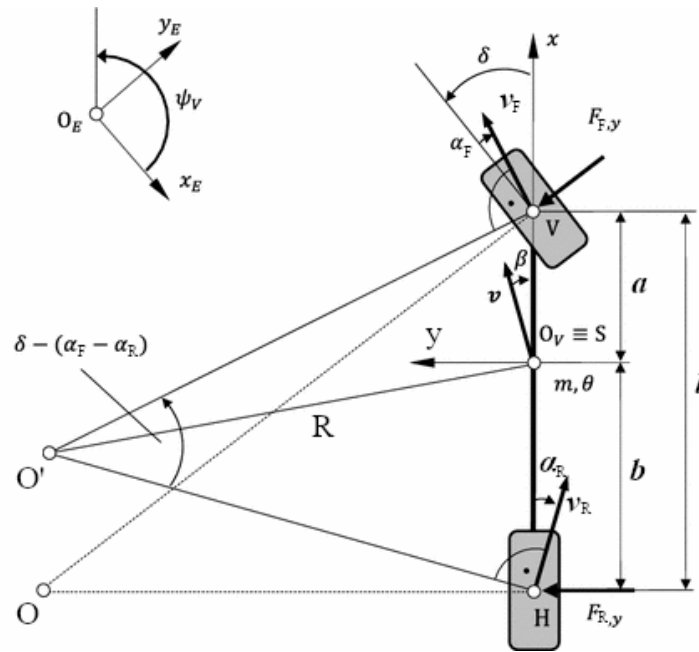


Figure 4.1.1 – Bicycle model.

The wheels in the same axle are collapsed into one equivalent wheel, so the model has one front wheel and one rear wheel. The simplifying hypothesis behind the model construction concerns the vehicle geometric modelling and its motion. The vehicle must move on a horizontal plane, with a constant speed. The steering angle  $\delta$ , as well as the side slip angle  $\beta$  and slip angles  $\alpha_F$  and  $\alpha_R$ , are almost null. The wheelbase length is negligible in respect to the radius of the curve path in which the vehicle is moving. The load transfer is neglected, and the axles behavior can be described with a linear relation. Under these hypotheses, the longitudinal and the lateral vehicle dynamics can be decoupled, and the vehicle behavior can be described by the slip angle of the front and the rear wheel, respectively  $\alpha_F$  and  $\alpha_R$ , the side slip angle  $\beta$ , the curve trajectory radius  $R$ , the yaw rate and the lateral acceleration. The aim of the test conducted is the acquisition of the lateral acceleration, the acquisition of the yaw rate and the acquisition of the wheel steering angle.

### 4.2 Steering models

The vehicle dynamics in a curve or, in general, during a steering condition, can be described with various models. Referring to the bicycle modelling of the vehicle, it is possible to distinguish two main steering model: the kinematic steering and the dynamic steering. The main difference between them is the introduction of the lateral forces contributes deriving from a different modelling of the wheels motion.

In the kinematic steering, the wheels roll without any slip, so the motion can be defined as a pure rolling motion. This implies that the slip angles are null and therefore also the lateral forces are null. There are only two conditions that make the lateral forces that should oppose to the centrifugal force null. The first is having a curve radius that tends to infinity, but in this case the vehicle is not moving in a curvilinear path anymore but in a linear one. The second is that the vehicle velocity has a very small value when moving in a curve. The kinematic steering model can be utilized in the study of a vehicle that moves at slow velocity when the inertial contribution on the lateral dynamic can be neglected. An example of this situation can be the parking maneuver.

In the dynamic steering a more realistic approach is used in the model definition with the introduction of the slip angles. This condition implies the introduction of the lateral forces, that must be studied to define the vehicle motion during a steering. In this model the system kinematic study is no more sufficient to describe the vehicle motion, but the dynamic equilibrium is needed to be investigated.

### 4.3 Triaxial Accelerometers

Triaxial accelerometers provide simultaneous measurements in three orthogonal directions, for analysis of all the vibrations being experienced by a structure. Each unit incorporates three separate sensing elements that are oriented at right angles with respect to each other [10]. The sensing element provides an acceleration value in the corresponding direction, identified as “x-direction”, “y-direction” or “z-direction”. The accelerometers used are the PCB Piezotronics 356A24 in Figure 4.3.1, a triaxial accelerometer having the following property (Table 4.3.1):

Table 4.3.1 – Accelerometer datasheet.

Dimension	Value
Sensitivity [mV/g]	( $\pm 15\%$ )10
Measurement range [g pk]	$\pm 500$
Measurement range [ $\text{m/s}^2$ pk]	$\pm 4905$



Figure 4.3.1– PCB Piezotronics 356A24.

The accelerometer has 8-36 4-pin connection thanks to which can be connected to an acquisition system. The acquisition system chosen is the SCADAS XS.

The aim of the test carried out with the accelerometers is to collect acceleration data that can be utilized for the understandings of the vehicle dynamics. The problem associated with these accelerometers is that are not capable to measure constant acceleration. This means that those accelerometers are not the best option for measure of the maximum vehicle acceleration, or deceleration. For the same reason, lateral vehicle dynamic could be a critical aspect to investigate with this equipment.

Beside the intrinsic limits of the triaxial accelerometers, a deeper study on the vibration the vehicle is subjected could be interesting for various reasons. One of this reason could be the characterization of the engine influence on the accelerations acquisition, or the influence that the external factors have on the measure.

#### **4.3.1 RPM estimation.**

One of the main problems for our vehicle dynamics test, is the engine vibration contribution on the chassis. This vibration contribution should be eliminated to analyze the vehicle dynamics. Ideally, knowing the instantaneous value of the engine RPM, it is possible to isolate and eliminate this contribution. However, the Losi 5ive-T 2.0 doesn't have a tachometer by which directly acquire the engine RPM, so an indirect way to derive the engine vibration on the chassis is needed. In addition, it is not possible to directly measure this information by installing a mechanical tachometer, because of the vehicle construction.

However, indirect ways exist. The first indirect way is to buy RPM sensors specifically intended for the Losi car models. Unfortunately, those sensors only work with electric engine car models. A second indirect way is to buy a digital tachometer that uses the Hall effect. These tachometers have Hall proximity switch sensors that allows to identify the electric current used for the spark plug. The sensor wires must be rolled around the spark plug cable so that with the magnetic inductance it is possible to detect the electric current flowing and from that derive the RPM value needed. The problem with this method is that the data cannot be easily read or stored in a memory; the rpm value is only displayed by the tachometer. A third way uses a Matlab function called "*rpmtrack*" and is the one discussed in the following paragraphs.

##### **4.3.1.1 The performed test**

The aim of this test is to collect data useful for the understanding of the vibrations to which the chassis is subject and create a post-processing algorithm that will be used for the vehicle dynamics study. The result wanted is to obtain the engine vibration contribution on the chassis using accelerometers and eliminate this contribution in the data collected.

In these tests, the RPM are estimated using Matlab *rpmtrack*.

The vibration data are acquired by four accelerometers, placed in the four corners of the chassis, and collected with the SCADAS XS. The Figure 4.3.1.1.1 shows the positions chosen for the accelerometers on the Losi 5ive chassis.

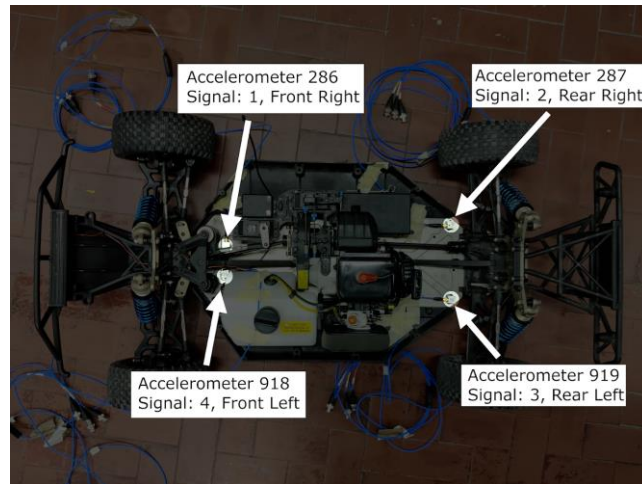


Figure 4.3.1.1.1 – Accelerometers.

The tests are performed in three Politecnico di Torino surroundings zone. The Zone 1 corresponds to Corso Castel Fidardo cycle path, the Zone 2 is the parking lot near to Politecnico Aule P, the Zone 3 is collocated between Aule P and the Thermal Power Station "Politecnico". All the three zones are plotted in Figure 4.3.1.1.1.

Forty-four tests have been conducted, from which five most representative ones have been chosen, i.e., the tests 13, 18, 22, 32 and 33. The Test 13 is performed in the Zone 1, the Tests 18 and 22 in the Zone 2, the Tests 32 and 33 in the Zone 3. With the aim to obtain a case study as general as possible, the tests are performed in different manners. During the Test 13 are collected data following a linear path; from the test 18 and above, the focus was on the acquisition of vehicle lateral acceleration, so a series of turns in sequence have been foreseen thanks to the use of delimiters pins.

During this phase the choose of the path doesn't affect the RPM results because of the relative low frequency the car can accelerate in different directions. The engine acceleration contribution on the chassis is way higher than the ones the car dynamics impose; what is expected are coherent RPM estimation among the various tests.

In the following figures are shown the routes the vehicle has taken.

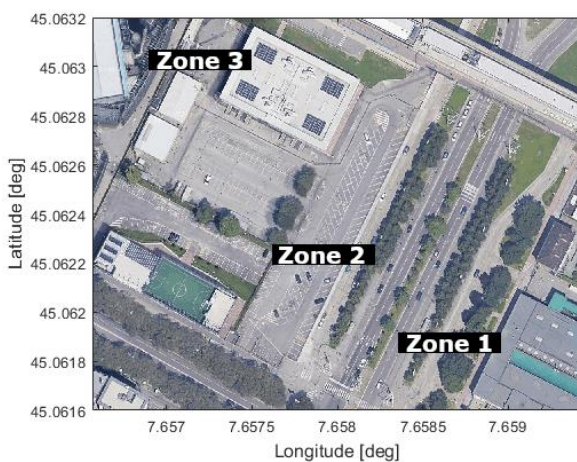


Figure 4.3.1.1.2 – Zone Test.

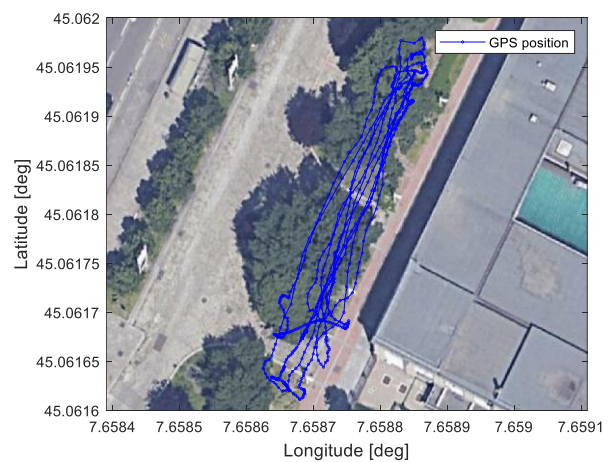


Figure 4.3.1.1.3 – Test 13.

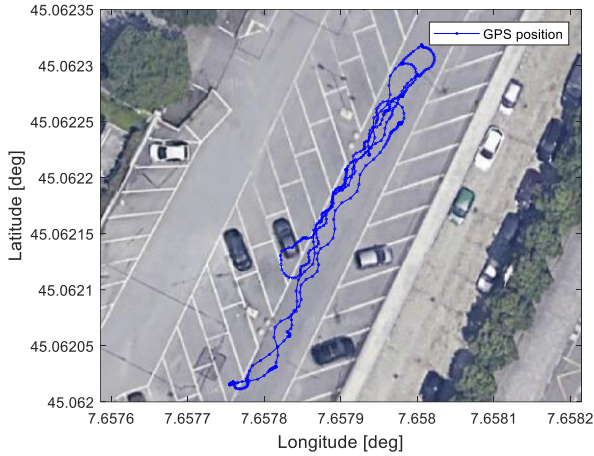


Figure 4.3.1.1.4 – Test 18.

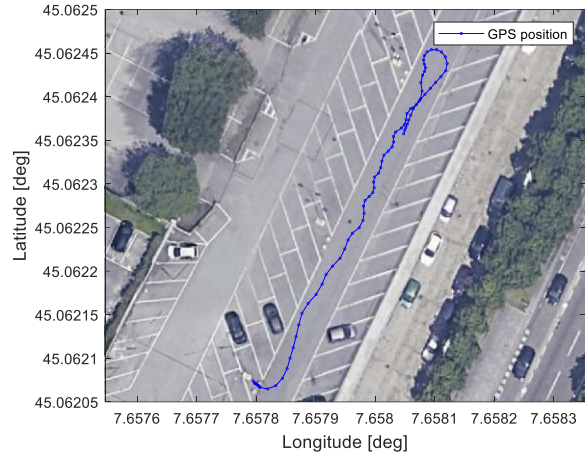


Figure 4.3.1.1.5 – Test 22.

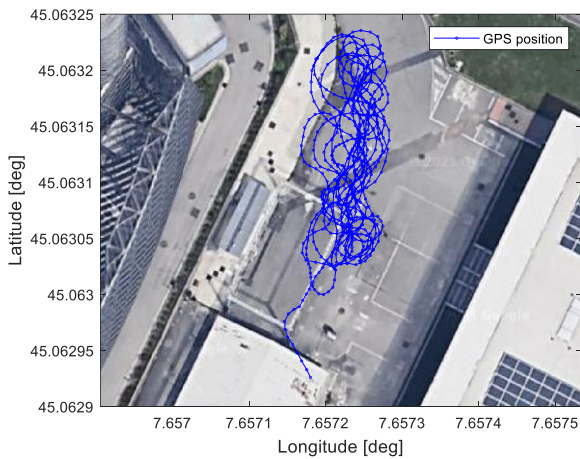


Figure 4.3.1.1.6 – Test 32.

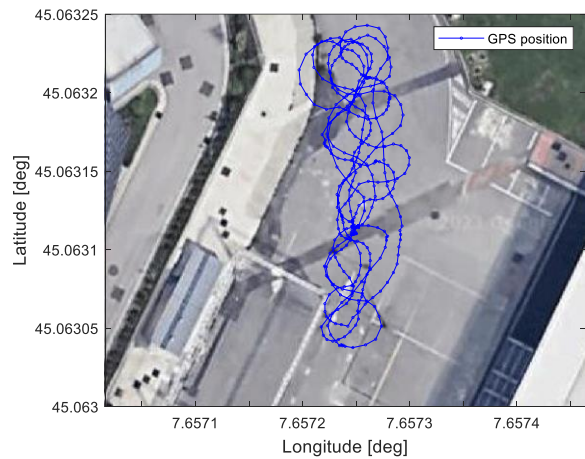


Figure 4.3.1.1.7 – Test 33.

### 4.3.1.2 Matlab “rpmtrack”.

The Matlab function *rpmtrack*, tracks and extracts RPM profile from vibration signal. It returns a time-dependent estimate of the rotational speed from a vibration signal. Please note that this function is not included in the standard Matlab installation, but the implementation of the Signal Processing Toolbox is needed.

The idea behind this study is to process an already existing vibration signal acquired during previous tests. This is both an advantage and a disadvantage. It is an advantage because it is not necessary to perform other tests to obtain these new data and it is a disadvantage because of the position of the accelerometers and the vibration contributions to which the accelerometers are subject. Ideally, the accelerometer should be placed on the stator and no other vibration sources should be present. In our case the accelerometers are placed on the chassis and are subject to different vibrations sources. Therefore, the RPM estimation will not be very accurate being affected by many contributions. As example, one of the contributions is the discontinuity of the ground in which the vehicle moves.

Having mounted four accelerometers on the chassis, *rpmtrack* will give four RPM curves. The curves should be in the range of 4 000 rpm to 20 000 rpm, values that come from the Zenoah G320 engine user manual [11].



During the tests, the throttle is pushed all the way down only few times, and therefore low RPM values are expected. What comes from the RPM estimation is that the engine works slightly under the 1 000 rpm at idle and arrives near to the 20 000 rpm with the throttle completely pushed. The RPM values during the vehicle runs ranges from 2 000 rpm to 4 000 rpm.

The clearer test result is obtained for the Test 13 (Figure 4.3.1.1.3). During this test, the vehicle mostly moves on a linear path and often is at idle; in addition, rapid accelerations are imposed with the throttle short time activation. The curve shows this trend. When the RPM value rise, there is also an increase of the speed values, while when the vehicle is at idle, the speed decreases almost linearly in time.

Note that the pseudo linear decrease of the speed is not associated to a constant value of the acceleration for a specific reason, i.e., the accelerometers property. In fact, the accelerometers used cannot acquire a constant value of acceleration but can detect with a high precision the change of acceleration. This is a great limit for them when utilized to acquire vehicle dynamics parameters and therefore an IMU is preferred in this specific application field.

The following graphs show the speed coming from the GPS speed depurated from the up velocity, as already explained in chapter 2, and the RPM estimation of each test. For a clearer reading of the graphs, only one most representative RPM curve will be plotted. In fact, since has been utilized four accelerometers, four RPM estimations are computed; in addition, not all the four estimation gives the same results due the unfavorable test conditions. However, it is possible to choose the most representative curve for the RPM estimation considering a common behaviour of the curves and the speed data coming from the GPS. In the following plots the four rpm curves are identified by a numeric value; in particular, the 1 identifies the accelerometer 286 front right, the 2 the accelerometer 287 rear right, the 3 the accelerometer 919 rear left, and lastly, the 4 identifies the accelerometer 918 front left.

Let's consider the rpm estimation coming from the Test 33 shown Figure 4.3.1.2.1.

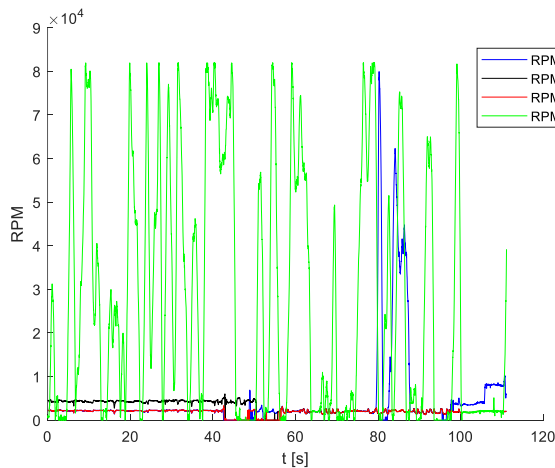


Figure 4.3.1.2.1– RPM estimation, Test 33.

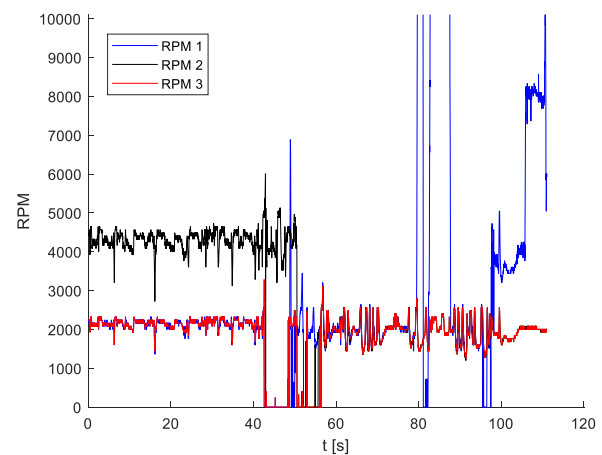


Figure 4.3.1.2.2– Zoomed view.

The estimation results show critical difference between the accelerometers signal, both in the numeric values and in the curve trend. The “RPM 4” is the result that the most differentiate from the others. It shows RPM values that have huge oscillations between the zero and the 80000 rpm. Considering the limits reported in the Zenoah engine, those results are completely out of range of the possible engine RPM values. For the same reason, also the “RPM 1” estimation cannot be considered, even if it shows a common trend with the other RPM estimations for most of the time.

The two remaining possibilities are the “RPM 2” curve or the “RPM 3” one. The choice between the two is suggested by the Figure 4.3.1.2.2, in which the “RPM 4” contribution has been deleted. In the plot it is possible to notice a common behaviour between the “RPM 1” and the “RPM 3” till

the second 80 of the tests, except for the seconds near the 50 seconds in which the “RPM 1” has an unexpected behaviour. The “RPM 2” instead has a completely different trend for the first 50 seconds, reporting values in the range of the 4000 rpm. After the 50 seconds, the “RPM 2” gives the same behaviour of the “RPM 3”. The “RPM 3” is the one that has, for the whole test time, a behaviour consistent with other rpm estimation. The final validation of this choice can be conducted analyzing the speed data coming from the GPS for the Test 33 in comparison with the vehicle speed, shown in Figure 4.3.1.2.3.

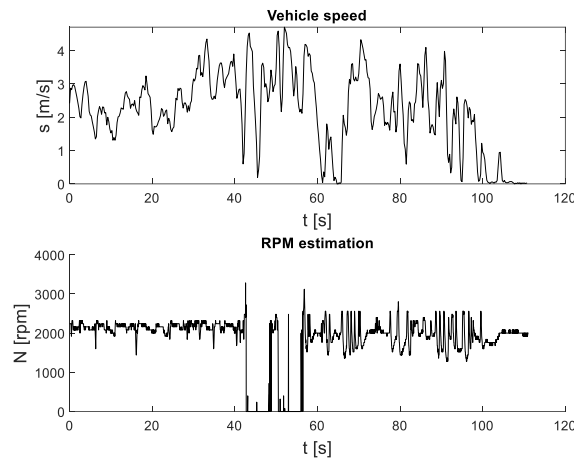


Figure 4.3.1.2.3– Test 33, speed and rpm comparison.

The estimation shows that to the rpm oscillation are associated speed value oscillation. There are some major issues for the results, i.e., the zero rpm value associated to a not null speed in the time range that goes from 40 seconds to 60 seconds. This is clearly an estimation error that, however, does not shows only in the “RPM 3” results, but appears also in the “RPM 2” and “RPM 1” in the same time range. Similar studies are performed on the other tests, where the rpm estimations coming from the four accelerometers have major differences between them, as happened for the Test 33, and estimations in which the rpm results are almost consistent, as happened for the Test 22. In Figure 4.3.1.2.4 are shown the rpm estimation coming from the Test 22.

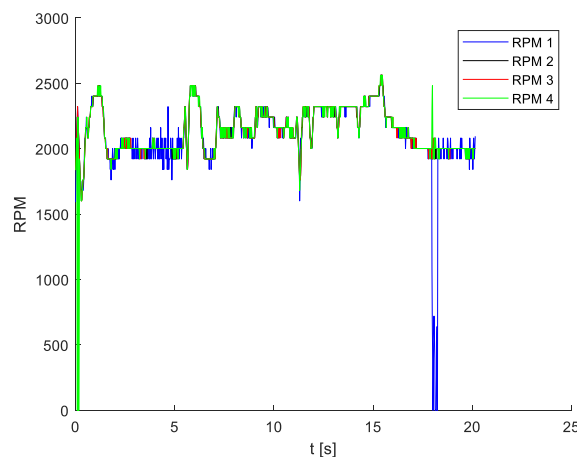


Figure 4.3.1.2.4– Test 33.

In the Table 4.3.1.2.1 are reported the RPM curve selected for each test.

Table 4.3.1.2.1 – RPM result selection.

Test	RPM curve selected
13	4
18	4
22	4
32	2
33	3

In the following figures are reported the RPM estimation plotted with the corresponding test speed.

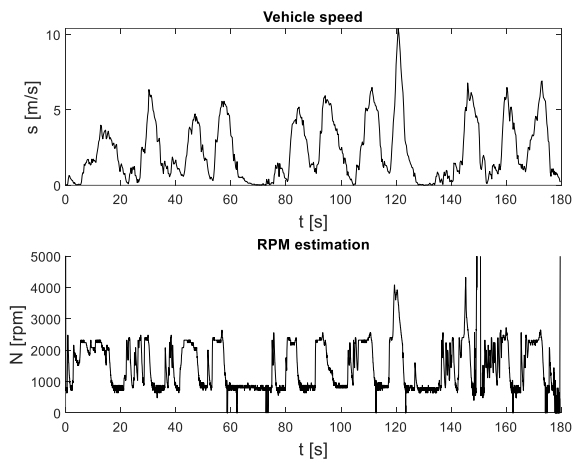


Figure 4.3.1.2.5– Test 13.

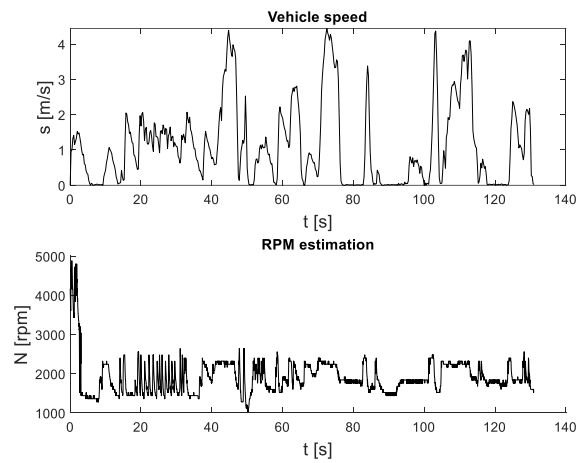


Figure 4.3.1.2.5 – Test 18.

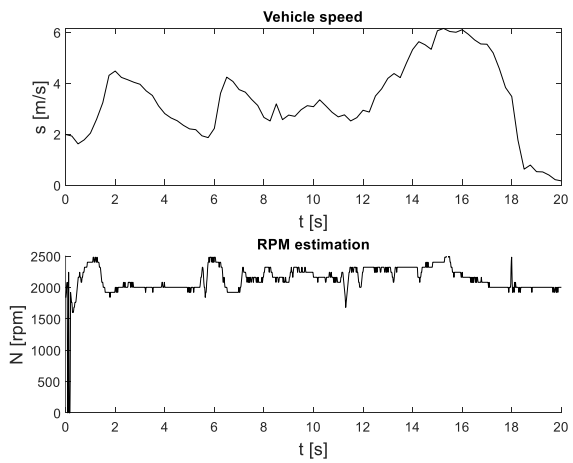


Figure 4.3.1.2.6 – Test 22.

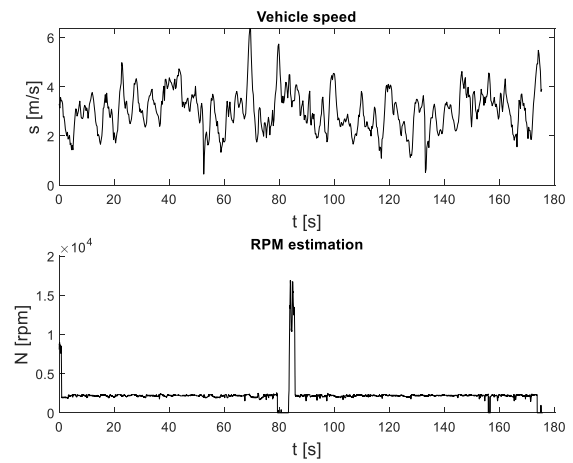


Figure 4.3.1.2.7 – Test 32.



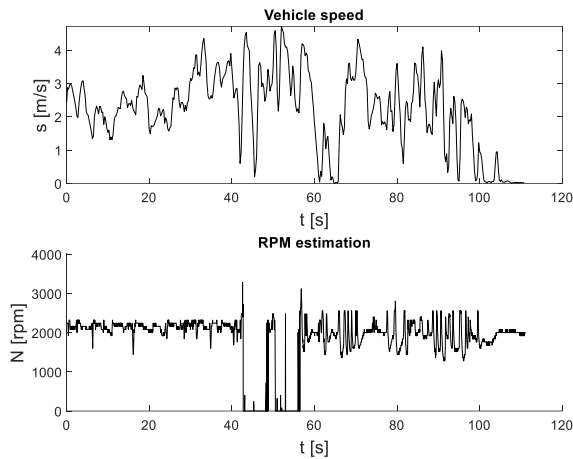


Figure 4.3.1.2.8 – Test 33.

### 4.3.1.3 RPM estimation results

As expected, the RPM curves have a behaviour that is coherent with what experienced during the tests acquisitions but are not precise in the numeric values. The user manual [11] gives the correct engine RPM values at idle and at maximum speed.

A rapid study of the manuals provided shows the following specifications:

Table 4.3.1.3.1 – Zenoah G320 32cc engine specifications.

Item	Value
Idling speed [rpm]	4000
No load maximum speed [rpm]	20000
Clutch engagement speed [rpm]	6000

Therefore, it is not possible to retrieve significant data by the means currently available, although the rpm test results are comparable with typical rpm value of a same size engine.

## 4.4 IMU

The last tests on the Losi 5ive-T 2.0 are performed with the aim to retrieve the lateral and longitudinal vehicle acceleration. Those data will be utilized together with the wheel steering angle and the vehicle speed information to perform a more in deep vehicle dynamics study.

The IMU utilized for the test is a SBG Ellipse-A, a high-performance MEMS based Inertial System. It is an equipment that can measure with high precision the orientation and the navigation performance of the system in which is mounted, and it is composed by an Inertial Measurement Unit running an on-board Extended Kalman Filter (EKF) [12]. The sensors the IMU utilize are three: three MEMS accelerometers, three MEMS gyroscope, and three anisotropic magneto-resistive magnetometers. The MEMS accelerometers record data about the accelerations in three perpendicular directions, namely the xyz IMU reference system; the three MEMS gyroscope are utilized to acquire the vehicle yaw, pitch, and roll; the magnetometers retrieve data about the orientation of the vehicle.

The SBG Ellipse-A IMU is shown in Figure 4.4.1, Figure 4.4.2, and Figure 4.4.3.



Figure 4.4.1 – IMU, isometric view.

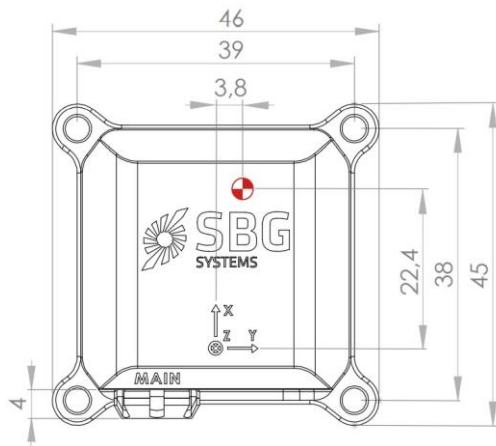


Figure 4.4.2 – IMU, dimensioned top view.

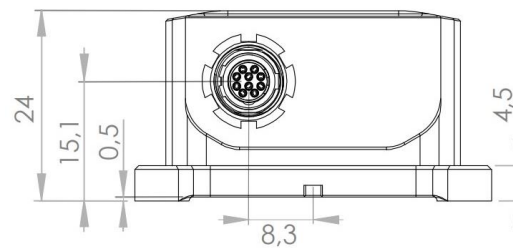


Figure 4.4.3 – IMU, dimensioned front view.

The IMU will be connected to the SCADAS XS via CAN connection and will be powered by the same Li-Po battery presented in the paragraph 3.5. The cable utilized for this connection has the IMU main connector plug on one side and has a derivation in the other cable side in which converge the IMU alimentation cable and the DB9 connector. The alimentation cable has two banana plug that must be connected to the battery; the DB9 connector must be connected to a DB9 to LEMO connector to be utilized with the SCADAS XS.

#### 4.4.1 IMU positioning on the vehicle

The place choice for the IMU positioning must guarantee protection to the sensor, must be as much stable as possible, and must allow the IMU to be integral with the vehicle body. The IMU is positioned on an aluminum plate mounted on the chassis in the rear part vehicle as shown in Figure 4.4.1.1.

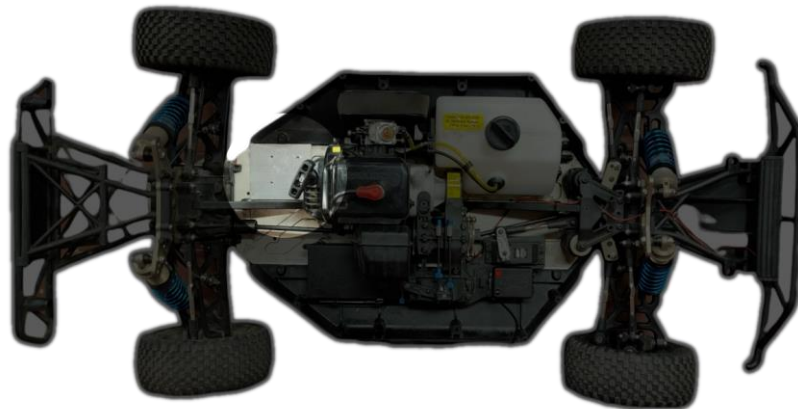


Figure 4.4.1.1 – IMU positioning.

The place evidenced in Figure 4.4.1.1 was the only one available that could guarantee the IMU to be integral with the vehicle and at the same time be stable. The problems with the position chosen are the heat and the possible presence of oil, gasoline, or dust particles due to the closeness with the engine. The issues are solved using a Vimar VIW14902 enclosure (Figure 4.4.1.2) for outdoor electric plug. This enclosure has an IP55 rating, meaning that is perfect to avoid the infiltration of unwanted particles, and is realized in a thermoresistant plastic material that protects the IMU from the heat. Note that the IMU itself has an IP68 rated resistance, the enclosure protection has been considered to give an extra protection for the sensor preservation.

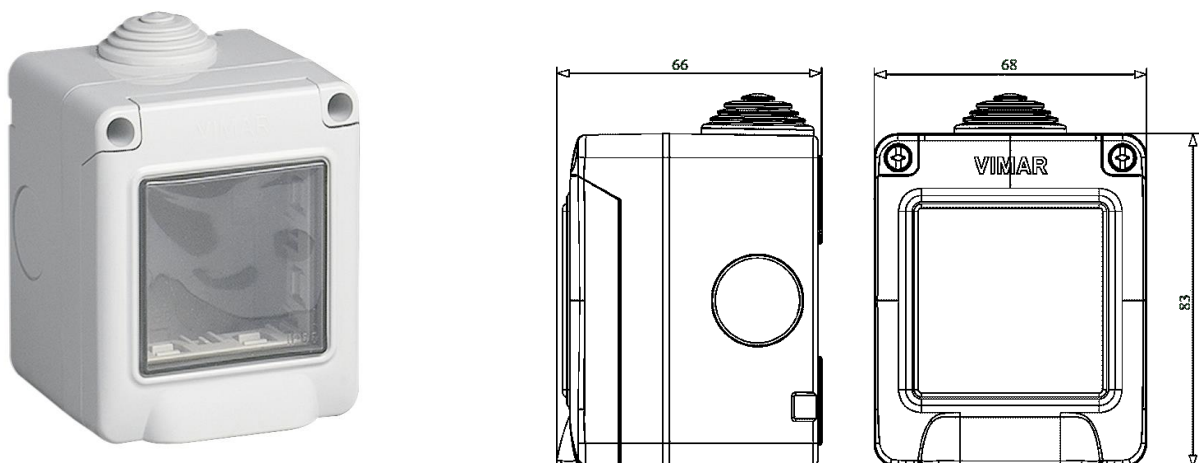


Figure 4.4.1.2 – Vimar VIW14902.

The lower half of the enclosure has been drilled to obtain four  $\phi 4 \text{ mm}$  holes allowing the mounting of the IMU and at the same time to secure the enclosure to the aluminum plate. In Figure 4.4.1.3 are represented the aluminum plate, the enclosure positioning on the aluminum plate and the IMU positioning in the enclosure.



Figure 4.4.1.3 – Left: the aluminum plate with the connection hole.  
Middle: the enclosure position on the aluminum plate.  
Right: the IMU mounted on the enclosure

The IMU is positioned paying attention to make the IMU input port coaxial with the cable port of the enclosure (Figure 4.4.1.4).



Figure 4.4.1.4 – View of the IMU input port coaxially in respect to the enclosure cable port.

Once the IMU is secured in the enclosure on the aluminum plate, the enclosure is closed with the upper part and the whole system is mounted on the chassis with three M5 screws, in the spot identified earlier utilizing already existent holes and vehicle elements for the installing. In Figure 4.4.1.5 and Figure 4.4.1.6 is shown the final installing.



Figure 4.4.1.5 – IMU final set up, top view.



Figure 4.4.1.6 – IMU final set up, lateral view.

With this set up is possible to connect the IMU to the SCADAS XS through the corresponding cable without the system disassembling. The IMU can remain mounted and can be connected only when needed.

Note that during the tests the IMU cable is not positioned close to the engine as represented due to the engine heat.

#### 4.4.2 Test performed

Fifteen acquisitions have been performed in the Zone 2 represented in Figure 4.3.1.1.2. The acquisitions have been made to retrieve the vehicle maximum longitudinal acceleration, the maximum lateral acceleration, the vehicle speed.

The following figures shows the data acquired with the IMU for three representative tests. In particular, has been reported the lateral acceleration variation in time, longitudinal acceleration variation in time, the yaw angle variation in time and the yaw rate variation in time.

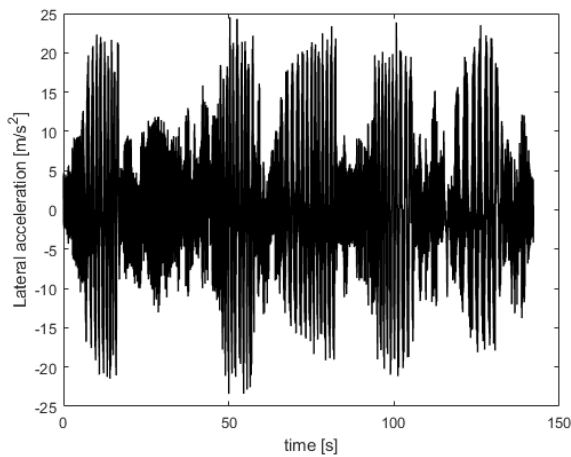


Figure 4.4.2.1 – Test 13.

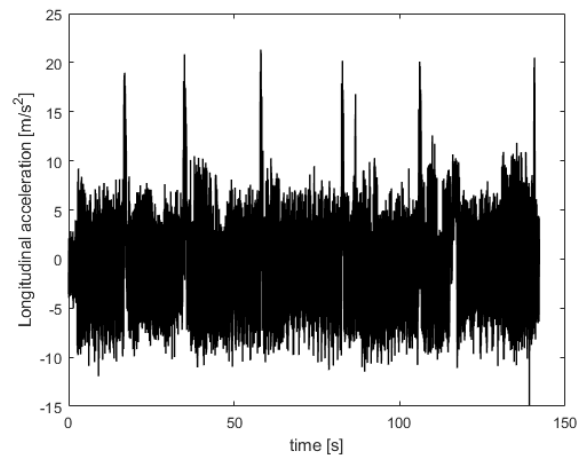


Figure 4.4.2.2– Test 13.

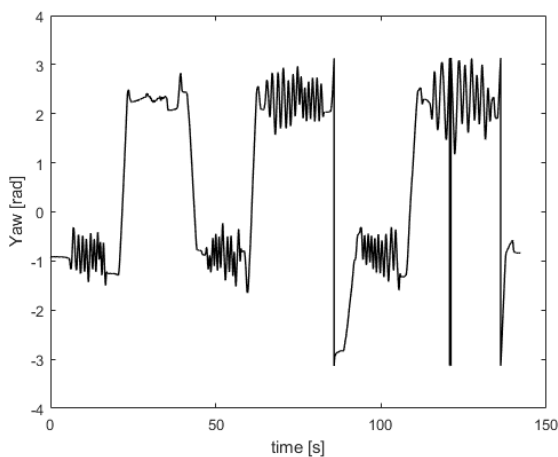


Figure 4.4.2.3 – Test 13.

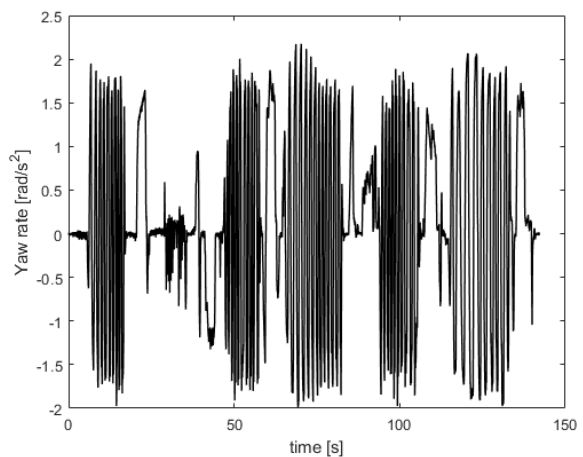


Figure 4.4.2.4 – Test 13.

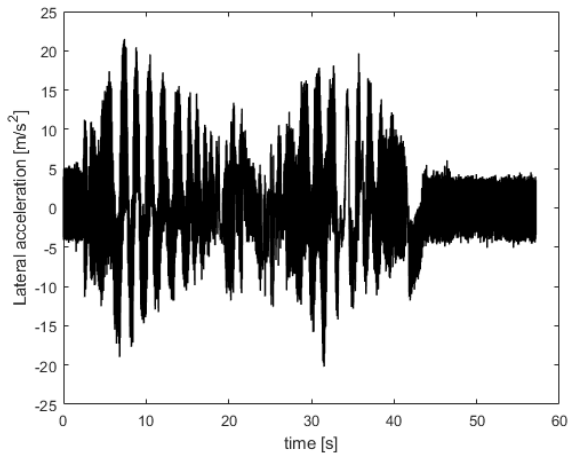


Figure 4.4.2.5 – Test 14.

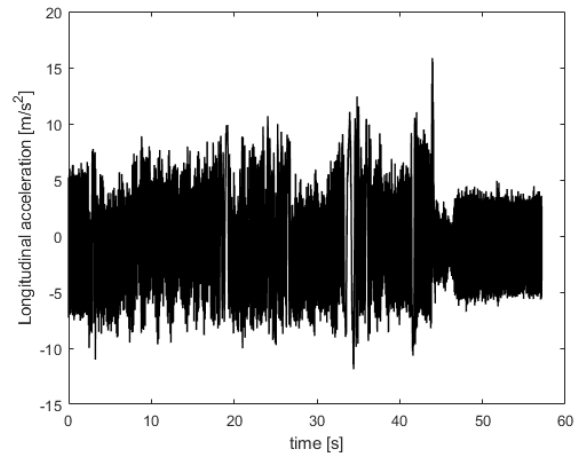


Figure 4.4.2.6 – Test 14.

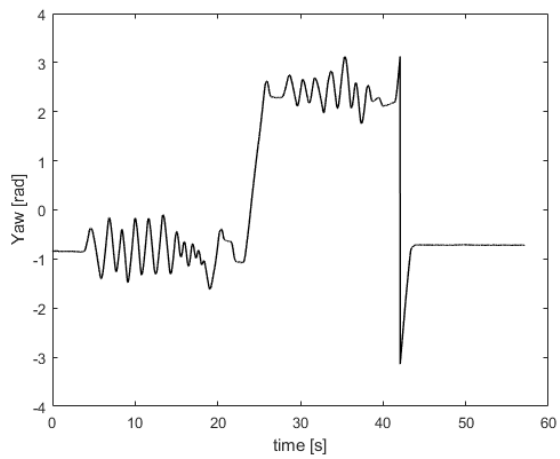


Figure 4.4.2.7 – Test 14.

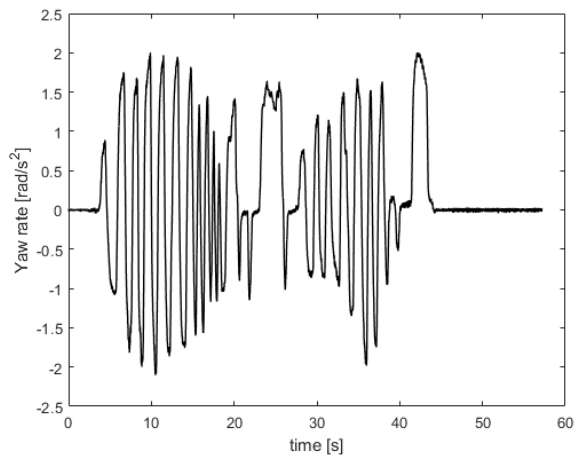


Figure 4.4.2.8 – Test 14.

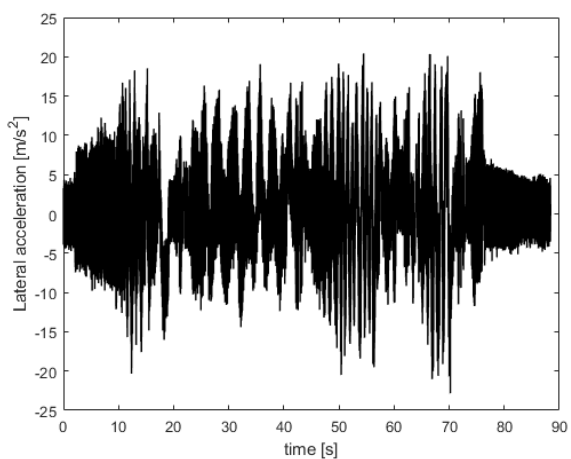


Figure 4.4.2.9 – Test 15.

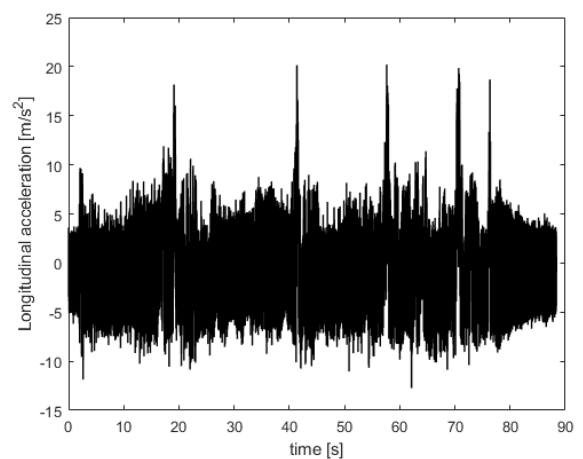


Figure 4.4.2.10 – Test 15.

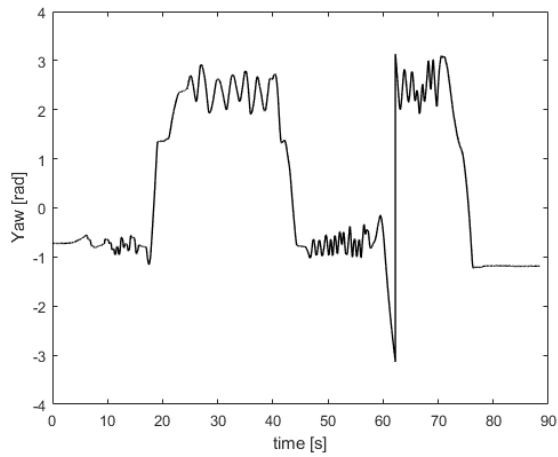


Figure 4.4.2.11 – Test 15.

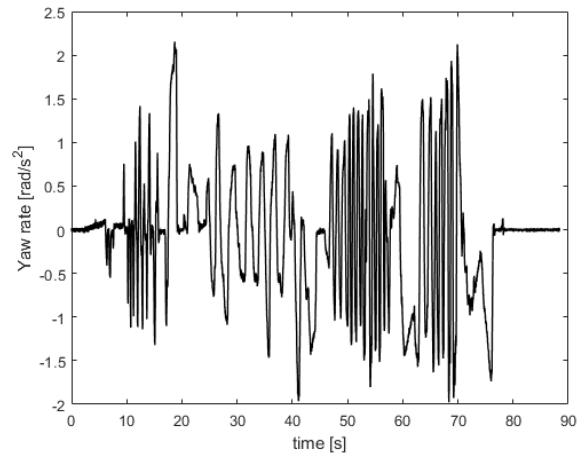


Figure 4.4.2.12 – Test 15.

Further investigations are needed for these data to describe the vehicle dynamics. The post process phase of this data set is not discussed in this thesis.

## 5 Conclusion and future development

In conclusion, in this thesis work have been investigated various experimental methods for the acquisition and the post process of vehicle dynamics data, namely the GPS data, the wheel steering angle, and the acceleration to which the vehicle is subject.

The post process of the GPS data involved a deep Matlab potentialities investigation, especially on the extended functionalities led by the Toolboxes, in this case the Mapping Toolbox. The Toolbox has been studied and compared with other distance and velocity computing methods to find a convergence of the results to take as reference. Moreover, the satellite map images has been retrieved by Google Maps thank to the utilization of the Google API. The GPS data analysis result is the built of a Matlab code that can extrapolate and plot the vehicle position in a satellite map, and can associate to the position various data, such as the speed, the total distance, and the orientation of the vehicle respect to the North pole and the East direction. The Matlab code, together with the Matlab function wrote and with the integration of Mapping Toolbox, represent a reliable base for future experimental analysis, not only related to the Losi 5ive-T 2.0, but for every experiment that involves the GPS utilization.

The experimental acquisition of the steering angle led to a different approach for the wheel angles acquisition. Generally, the scale vehicles have a set of sensors that shows in real time the vehicle parameters, such as the motor rpm, or the engine temperature, or again the tachometer information. This is partially true for the gasoline powered engine that lacks all the built-in control sensor the electric motors have. Considering that the wheel steering angle is not effortlessly measurable during the vehicle motion due to the element working conditions, an experimental alternative measure has been found in the measure of the servomotor rotation. After the mathematical modelling and the CAE modelling of the steering system, it has been possible to find the correlation between the rotation of the electric motor, that moves the steering system, and the wheel. The problem went from the measure of the wheel rotation to an easier rotation measure of a vehicle internal component. This rotation measure has been acquired thanks to an analog signal coming from a potentiometer, powered by a battery, linked to the servomotor. The result of this second experimental part of the thesis is the estimation of the wheel steering angle starting from an analog voltage input.

The last part of the thesis concerns the vehicle dynamics parameters acquisition and the wheel steering angle during the vehicle ride. The aim is now finding the right set up for the sensors to acquire the vehicle parameters. The sensor utilized for this last experimentation are the GPS, the steering acquisition potentiometer and an IMU connected via CAN to a Simcenter SCADAS XS. The tests conducted show a good behavior of the mounted sensors, testifying that the sensor system set up is reliable and gives consistent measures in respect to the expectations.

Future experimental analysis on the Losi 5ive-T 2.0 could be focused on the correlation of the vehicle steering angle with the longitudinal and lateral acceleration.



## Reference

- [1] <http://www.losi.com/Products/Features.aspx?ProdID=LOS05014T1> o meglio il manual? Available in 2021-11-30.
- [2] LOS05014-Manual-MULTI, 2018.
- [3] Pesacane F., *Numerical models and experimental measurements for parametric dynamic analyses on a vehicle in scale 1/5*, MSc Thesis, Politecnico di Torino, Torino, Italy, 2020.
- [4] Berco S.p.A. CM250E Istruzioni per l'uso e la manutenzione, [2001].
- [5] [https://en.wikipedia.org/wiki/Global\\_Positioning\\_System](https://en.wikipedia.org/wiki/Global_Positioning_System), available in 2021-11-30.
- [6] [https://en.wikipedia.org/wiki/Great-circle\\_distance](https://en.wikipedia.org/wiki/Great-circle_distance), available in 2021-11-30.
- [7] <https://www.ni.com/it-it/shop/pxi.html>, available in 2021-11-30.
- [8] <https://www.mscsoftware.com/product/adams>, available in 2021-11-30.
- [9] Schramm D., Hiller M., Bardini R., "Single Track Models", *Vehicle Dynamics. Springer, Berlin, Heidelberg*, 2014.
- [10] <http://www.pcb.com/sensors-for-test-measurement/accelerometers/general-purpose/triaxial>, available in 2021-11-30.
- [11] Husqvarna Zenoah Co., Ltd., G320rc Owner's Manual, 2018.
- [12] Ellipse 3 - Hardware Manual, [2020].